Age-related Islet Inflammation Marks the Proliferative Decline of Pancreatic Beta-cells in Zebrafish

Sharan Janjuha[1,2,6], Sumeet Pal Singh[1,6], Anastasia Tsakmaki[3], S. Neda Mousavy Gharavy[4], Priyanka Murawala[1], Judith Konantz[1], Sarah Birke[1], David J. Hodson[5], Guy A. Rutter[4], Gavin A Bewick[3] and Nikolay Ninov[1,2,7]

[1] Centre for Regenerative Therapies TU Dresden, Dresden 01307, Germany

[2] Paul Langerhans Institute Dresden of the Helmholtz Center Munich at the University Hospital Carl Gustav Carus of TU Dresden, Dresden 01307, Germany

[3] Diabetes Research Group, School of Life Course Sciences, Faculty of Life Sciences & Medicine, King's College London, London SE1 91UL,

[4] Section of Cell Biology and Functional Genomics, Division of Diabetes, Endocrinology, and Metabolism, and Consortium for Islet Cell Biology and Diabetes, Department of Medicine, Imperial College London, Du Cane Road, London W12 0NN, United Kingdom.UK

[5] Centre for Endocrinology, Diabetes, and Metabolism, and Institute of Metabolism and Systems Research, University of Birmingham, Edgbaston B15 2TT, United Kingdom

[6] Equal contributions

[7] Corresponding author: nikolay.ninov@tu-dresden.de

Abstract

The pancreatic islet, a cellular community harboring the insulin-producing beta-cells, is known to undergo age-related alterations. However, only a handful of signals associated with aging have been identified. By comparing beta-cells from younger and older zebrafish, here we show that the aging islets exhibit signs of chronic inflammation. These include recruitment of *tnfα*-expressing macrophages and the activation of NF-kB signaling in beta-cells. Using a transgenic reporter, we show that NF-kB activity is undetectable in juvenile beta-cells, whereas cells from older fish exhibit heterogeneous NF-kB activity. We link this heterogeneity to differences in gene expression and proliferation. Beta-cells with high NF-kB signaling proliferate significantly less compared to their neighbors with low activity. The NF-kB signaling^{hi} cells also exhibit premature upregulation of *socs2*, an age-related gene that inhibits beta-cell proliferation. Together, our results show that NF-kB activity marks the asynchronous decline in beta-cell proliferation with advancing age.

60 **Introduction**

61 Aging is a universal process that detrimentally changes the characteristics of cells in
62 all multicellular organisms. A hallmark of aging is the reduction in cellular renewal and
63 proliferation across different tissues and organs (Yun, 2015). The insulin producing beta-
64 cells, which reside in the islets of Langerhans, provide a good model to study regulators of
65 cellular aging. Whereas young beta-cell are highly proliferative and increase rapidly in
66 number from the prenatal phase until early stages of development in mammals, beta-cell
67 proliferation becomes dramatically reduced in adults (Perl *et al*, 2010). Nevertheless, adult
68 beta-cell proliferation can increase under specific conditions such as obesity and pregnancy
69 (Parsons *et al.*, 1992, Weir *et al.*, 2001). It remains unclear whether this proliferation is
70 restricted to a privileged population of beta-cells that retain replicative potential even in adult
71 life, or whether it represents stochastic cell cycle re-entry.

72 Previous studies have indicated that both extrinsic factors, such as the vasculature, and
73 intrinsic factors, such as chromatin modifications, may influence the age-related changes in
74 beta-cells. For example, rejuvenating the beta-cell environment by implanting old islets in
75 younger animals is sufficient to restore the proliferative potential of the aged beta-cells
76 (Almaça *et al*, 2014, Salpeter *et al*, 2013). In addition, transcriptome and methylome studies
77 revealed age-dependent DNA methylation changes at cell-cycle regulators, which may
78 contribute to the quiescence of aging beta-cells (Avrahami et al., 2015, Arda et al., 2016).
79 Furthermore, analysis of gene expression in islets from aging mice showed an age-dependent
80 decline of transcripts encoding the platelet derived growth factor-receptors Pdgfra and Pdgfrb
81 as well as its ligand Pdgf. This decline in expression was shown to underlie a decline in beta-
82 cell proliferation with aging (Chen *et al.*, 2011). Likewise, the expression of the transcription
83 factor FoxM1 declines with aging and the forced expression of its activated form in aged beta-
84 cells is sufficient to re-ignite replication (Golson *et al.*, 2015). In addition, the prostaglandin

85 receptors (E-Prostanoid Receptor 3 and 4) might also regulate beta-cell proliferation in an
86 age-dependent manner (Carboneau *et al*, 2017).

87 An important aspect of beta-cell biology is the presence of significant heterogeneity
88 within a seemingly homogenous collection of cells. In partiuclar, beta-cells within the islet
89 and between islets may belong to subpopulations with different "ages" (Meulen *et al*., 2017,
90 Singh *et al*., 2017), with the proportion of young-to-old beta-cells changing with the age of
91 the animal (Aguayo-mazzucato *et al*, 2017). In addition, recent studies have identified
92 various markers of beta-cell hetereogeneity such as *Fltp*, ST8SIA1 and CD9 (Bader *et al*,
93 2016, Dorrell *et al*, 2016). Specifically, *Fltp* was shown to distinguish the proliferative beta-
94 cells from the more functional ones. However, the markers of beta-cell heterogeneity have
95 not yet been shown to play a direct role in establishing phenotypic differences among the
96 beta-cell subpopulations. In addition, it remains unclear how aging shapes the proliferative
97 heterogeneity of the beta-cells.

98 To identify signals that change in beta-cells during organismal aging, we used the
99 zebrafish as a model. We first characterized the rate of beta-cell proliferation in juvenile,
100 younger and older adults, and found that proliferation declines with advancing age. We
101 performed transcriptomics of beta-cells from younger and older animals, which identified an
102 upregulation of genes involved in inflammation, including NF-kB signaling. The analysis of
103 inflammatory signaling with single-cell resolution using a transgenic GFP reporter line
104 confirmed that NF-kB signaling was activated in a heterogeneous manner at the level of
105 individual beta-cells. Notably, beta-cells with higher levels of NF-kB signaling exhibit a
106 more pronounced proliferative decline compared to their neighbors with lower activity. These
107 cells also express higher levels of *socs2*, which can inhibit beta-cell proliferation in a cell-
108 autonomous manner. Our work identifies NF-kB signaling as a marker of beta-cell aging and
109 their proliferative decline.
110

111 **Results**

112 **Beta-cell proliferation declines with advancing age in zebrafish**

113 To monitor the endogenous rate of proliferation of zebrafish beta-cells, we used the
114 beta-cell specific fluorescence ubiquitination cell cycle indicator (FUCCI) lines,
115 *Tg(ins:Fucci-G1)* and *Tg(ins:Fucci-S/G2/M)* (Ninov *et al*, 2013). The FUCCI system uses
116 fluorescent proteins fused with CDT1 to label cells in the G0/G1 phases of cell cycle with red
117 fluorescence and GEMININ to label cells in S/G2/M with green fluorescence (Figure 1a). We
118 imaged whole primary islets from normally-fed fish at 35 days-post-fertilization (dpf), 3
119 months-post-fertilization (mpf) and 1 year-post-fertilization (ypf) (Figures 1c-e). We
120 calculated the percentage of *Tg(ins:Fucci-G1)*-negative and *Tg(ins:Fucci-S/G2/M)*-positive
121 cells among the total number of beta-cells per islet. We found that the percentage of
122 proliferating beta-cells declined with advancing age. Whereas in islets from 35 dpf animals,
123 on average 1.53% ± 0.72 (n=5) of the beta-cells were proliferating, this number was reduced
124 to 0.15% ± 0.07 (n=9) and 0.06% ± 0.02 in islets from 3 mpf and 1 ypf animals, respectively
125 (n=10) (Figure 1b). A similar decline in beta-cell proliferation was observed also in the
126 secondary islets, which arise from the differentiation of *sox9b*-expressing progenitors lining
127 the pancreatic ducts (Figure 1-figure supplement 1a-d).

128 To confirm that adult beta-cells within the zebrafish primary islets are functional, we
129 analyzed glucose-stimulated calcium influx using *Tg(ins:GCaMP6s)* transgenic line, a
130 genetically-encoded calcium indicator that binds to increasing intracellular Ca^{2+} and emits
131 green fluorescence (Singh *et al*, 2017). We crossed this line to *Tg(ins:nlsRenilla-mKO2)*,
132 which marks the beta-cells with red fluorescence. This double transgenic system allowed us
133 to visualize the response of beta-cells to increasing concentrations of glucose over time *ex*
134 *vivo* (n=10) (Figures 1f-f'''). We found that adult beta-cells were sensitive to glucose, as
135 beta-cells exhibited calcium spikes upon stimulation with increasing glucose concentrations.

136

137 **Aging is associated with transcriptional changes in zebrafish beta-cells**

138 To determine changes in gene expression in beta-cells with increasing age, we used
139 fluorescence-activated cell sorting (FACS) coupled with next generation RNA-Sequencing to
140 profile fluorescently-labelled beta-cells from 3 mpf and 1 ypf animals (Figures 2a-a', Figure
141 2-figure supplement 2a). We selected these two stages in order to avoid confounding changes
142 in gene expression associated with the morphogenesis and the remodeling of the islets
143 occurring during the juvenile stages (Singh et al., 2017). Thus, we compared the
144 transcriptomes of beta-cells at 3 mpf and 1 ypf to identify genes that increase in expression
145 with increasing age in the absence of active morphogenesis and rapid organismal growth. In
146 order to avoid introducing sequencing noise or bias, RNA-Sequencing of sorted beta-cells was
147 carried out without PCR amplification of the staring mRNA. A comparison between beta-
148 cells from 3 mpf and 1 ypf animals revealed 74 genes that showed 1.5-$\log_2$fold difference
149 ($p<0.05$) in expression (Figure 2b), of which 61 genes were upregulated and 13 genes were
150 downregulated in older beta-cells (Supplementary File 1). Literature survey and unbiased
151 gene ontology analysis using DAVID (Huang et al., 2009a, Huang et al., 2009b) revealed that
152 the upregulated genes were involved in the negative regulation of growth-factor signaling
153 including *socs2*, *cish*, *spry4* and *fstl1* (Figures 2c-c'). We also found upregulation of genes
154 involved in ER stress including *trib3* and *cebpd*, as well as genes associated with increased
155 risk of developing Type 2 diabetes and glucose intolerance (*prtfa*, *lpp* and *socs2*) (Fang et al.,
156 2014, Szabat et al., 2016, Kato et al., 2006, Lebrun et al., 2010, Nair et al., 2014, Liu et al.,
157 2008).

158 **NF-kB-signaling is activated heterogeneously in the beta-cells with advancing age**

159 In addition to the genes involved in regulating proliferation and ER stress, cytokine-
160 mediated signaling was over-represented in the gene ontology analysis performed using
161 DAVID (Figure 2c'). We found that transcripts associated with an inflammatory signature,
162 such as interleukins, complement factors and members of the NF-kB pathway, including *il15*,

163 *c9*, *tnfrsf1b*, *cd74a*, *cd74b* (Starlets *et al*, 2006), also increased in expression in islets from
164 older animals (Supplementary File 1). Specifically, *tnfrsf1b* belongs to a superfamily of
165 cytokine receptors, which respond to Tumor Necrosis Factor (TNF) and activate NF-kB, an
166 inducible and ubiquitous transcription factor that senses inflammation (Espı´n-Palazo´n *et al*,
167 2014). In order to validate the changes in gene-expression of *tnfrsf1b* at the level of
168 individual cells, we performed single-cell RT-qPCR of sorted beta-cells (Supplementary File
169 2). Notably, the single-cell RT-qPCR revealed that there was an increase in the proportion of
170 beta-cells expressing *tnfrsf1b* in islets of older animals (Figure 2d). This was also true for
171 additional components of the NF-kB pathway, including *ikbaa* and *tnfα*. In contrast, the
172 proportion of sorted cells expressing known beta-cell markers such as *insulin*, *islet1* and
173 *neurod1*, remained similar (Figure 2d).

174 We then wanted to test if overexpressing *tnfrsf1b* in beta-cells can induce NF-kB
175 signaling. To do so, we cloned *tnfrsf1b* in a plasmid containing an upstream insulin promoter
176 and injected it into one-cell-stage embryos. The ensuing stochastic genomic integration and
177 expression from the insulin promoter leads to mosaic overexpression of *tnfrsf1b* specifically
178 in beta-cells. We analyzed the activity of NF-kB using an NF-kB signaling reporter line,
179 *Tg(NF-kB:GFP)* (Kanther *et al*, 2011). This reporter expresses GFP under the control of six
180 tandem NF-kB binding sites, such that GFP is expressed upon the nuclear translocation and
181 binding of NF-kB dimer to the NF-kB binding sites. We saw that a higher proportion of beta-
182 cells from animals injected with *ins:tnfrsf1b* expressed GFP at 5 dpf compared to controls. A
183 total of 32.2 % ± 32.07 beta-cells (n=6) in the *tnfrsf1b*-injected animals expressed GFP as
184 compared to 2.4 % ± 1.98 beta-cells (n=5) in the controls (Figures 3a-b).

185 The ability of *tnfrsf1b* overexpression to activate NF-kB signaling and the increase in
186 the proportion of beta-cells that upregulate *tnfrsf1b* with age (Figure 2d) prompted us to
187 follow-up on the endogenous levels of NF-kB signaling in the beta-cells. We performed a
188 temporal analysis of NF-kB activity in beta-cells by imaging the islets from *Tg(NF-kB:GFP)*

189 animals (Figures 3c-e, Figure 3-figure supplements 1a-d). We found that GFP intensity was
190 too low to be detected in the primary or secondary islets from juveniles (1 mpf) (Figure 3c,
191 Figure 3-figure supplement 1a). In contrast, beta-cells from 3 mpf animals exhibited a
192 detectable, salt-and-pepper pattern of GFP expression (Figure 3d, Figure 3-figure supplement
193 1b), suggesting heterogeneous NF-kB activation, which is consistent with the heterogeneous
194 expression of *tnfrsf1b* (Figure 2d). Notably, nearly all beta-cells in both the primary and
195 secondary islets from 1 ypf animals express GFP (Figure 3e, Figure 3-figure supplement 1c).
196 To better quantify the proportions of GFP-positive cells in younger and older islets, we
197 labelled beta-cells from 3 mpf and 1 ypf *Tg(NF-kB:GFP)* animals using the Zn^{2+} chelator
198 TSQ (Kim *et al*, 2000), which preferentially labels beta-cells due to their high zinc content
199 (Figure 3-figure supplements 2a-b). TSQ-labelled beta-cells were then passed through FACS
200 and were analyzed for the levels of GFP expression in each cell. Flow cytometry analysis of
201 cells from 3 mpf and 1 ypf animals confirmed the presence of two populations at each stage
202 based on GFP-fluorescence intensity (Figures 3f-g) (n=10). Quantifying the proportion of
203 cells within the low- and high-GFP expressing regions indicated that a higher proportion of
204 cells express GFP in older animals (Figures 3f-g). Thus, we found that not only does the
205 overall GFP expression increases in individual cells with increasing age, but a higher
206 proportion of cells with GFP expression were present in the islets of the older compared to
207 younger animals (Figures 3f-g).
208 In order to verify that the increase in GFP levels in older fish is not simply due to the
209 accumulation of GFP protein, we quantified using RT-qPCR the differences in GFP mRNA in
210 beta-cells sorted from 3 mpf and 1 ypf animals of the genotype *Tg(ins:mCherry);Tg(NF-*
211 *kB:GFP)*. We saw a 50% increase in the GFP transcript levels in beta-cells from 1 ypf
212 animals as compared to 3 mpf animals (Figure 3-figure supplement 3a). This result
213 corroborates the increase in NF-kB reporter activity in beta-cells between the two time points.
214 Furthermore, we used index sorting of single-cells, which allows to correlate transcript levels

215 with GFP fluorescence intensity in individual beta-cells. Overall, there was a positive
216 correlation between GFP mRNA and GFP fluorescence intensity across cells ($R^2 = 0.28$)
217 (Figure 3-figure supplement 3b).

218 **Immune cells infiltrate the islet during development and persist throughout adult life**

219 An enrichment of genes associated with an inflammatory signature in beta-cells from
220 older fish together with the heterogeneous activation of the NF-kB pathway prompted us to
221 look for additional signs of islet inflammation. One cell type important for the response and
222 resolution of inflammation is the tissue-resident macrophage. To study this cell type in the
223 developing islet, we labelled immune cells using a pan-leukocyte marker, L-plastin, which
224 marks the monocyte/macrophage lineage in zebrafish (Mathias *et al*, 2010). We found that
225 whereas innate immune cells were not present in the islets during the larval stages (15-21
226 dpf), they had infiltrated them during the late juvenile stages (45 dpf) (Figure 4a). Analysis of
227 the macrophage reporter line, *Tg(mpeg1*:mCherry*)*, revealed that the innate immune cells
228 were macrophages, whereas neutrophils could not be detected, as assessed by the neutrophil
229 specific line *Tg(lyz2:GFP)* (Figure 4-figure supplement 1a, data not shown).

230 To test whether these infiltrating immune cells express inflammatory cytokines, such
231 as TNFα, we made use of a *TgBAC(tnfα:GFP)* transgenic line and examined the presence of
232 *tnfα*-expressing leukocytes within the L-plastin-positive population (Marjoram *et al*, 2015).
233 On average 25% ± 10.9 (n=5) and 17% ± 11.1 (n=5) of the L-plastin positive cells inside the
234 islet expressed *tnfα:*GFP in 3 mpf and 1 ypf animals, respectively ($p > 0.05$) (Figure 4b, Figure
235 4-figure supplement 1b). However, the number of *tnfα*:GFP-positive cells, as well as the total
236 number of L-plastin-positive cells showed increasing trends in the islets from older animals
237 (Figure 4-figure supplement 1c-d). Analysis of *TgBAC(tnfα:GFP)* together with specific
238 labeling of macrophages using *Tg(mpeg1:mCherry)* confirmed that the *tnfα:*GFP-expressing
239 leukocytes were macrophages (Figure 4c).

240 We next wanted to test whether TNFα is capable of inducing inflammatory activity in
241 the beta-cells. To this end, we placed *tnfα* under the insulin promoter in order to drive beta-
242 cell specific expression. We injected the construct in one-cell-stage *Tg(NF-kB:GFP)* embryos
243 and analyzed GFP-expression in beta-cells at 5 dpf. Indeed, we found that TNFα alone could
244 induce *NF-kB*:GFP reporter expression (Figures 4d-e).

245 ***NF-kB*:GFP^{high} beta-cells proliferate less compared to their neighbors**

246 Based on the earlier observation that beta-cell proliferation declines in older fish, and
247 the finding that *NF-kB*:GFP expression increases, we asked if high NF-kB activity and beta-
248 cell proliferation were inversely correlated. We performed 5-ethynyl-2´-deoxyuridine (EdU)
249 incorporation assay to mark the proliferating beta-cells in 3 mpf *Tg(NF-kB:GFP)* animals and
250 examined the levels of *NF-kB*:GFP in the EdU-positive and negative beta-cells. We measured
251 the normalized GFP intensity in all beta-cells in the islets of 3 mpf animals (n=9). The total
252 normalized mean GFP intensity of all the sections belonging to one islet, designated GFP^{total},
253 was set as a threshold for each respective islet. The beta-cells with normalized mean GFP
254 intensity higher than GFP^{total} were categorized as *NF-kB*:GFP^{high} while cells with normalized
255 mean GFP intensity lower than GFP^{total} were categorized as GFP^{low}. We observed that a
256 lower proportion of the *NF-kB*:GFP^{high} cells had incorporated EdU over a two-day period as
257 compared to GFP^{low} cells (Figures 5a-c). In order to confirm that the GFP fluorescence of
258 beta-cells remains stable over the two-day period of EdU incorporation, we followed
259 individual FAC-sorted *NF-kB*:GFP^{high} and ^{low} beta-cells over 72 hours ex vivo. Indeed, the
260 GFP fluorescence remained stable over the time-period of the experiment (Figure 5-figure
261 supplement 1). In addition, to obtain a snapshot of the proliferative status of the cells, we
262 performed immunohistochemistry for the proliferating cell nuclear antigen (PCNA), which
263 marks proliferating cells. A higher proportion of *NF-kB*:GFP^{low} cells were positive for
264 PCNA, as compared to *NF-kB*:GFP^{high} cells (Figure 5d, Figure 5-figure supplement 2). We

265 conclude that beta-cells with high NF-kB signaling proliferate significantly less compared to
266 their neighbors with lower activity.

267 ***Socs2* is enriched in *NF-kB*:GFP^{high} beta-cells and inhibits proliferation**

268 To investigate molecular factors to explain the lower proliferation of *NF-kB*:GFP^{high}
269 beta-cells, we separated the beta-cells from 3 mpf animals into GFP^{high} and GFP^{low}
270 populations using a double transgenic line *Tg(ins:mCherry);Tg(NF-kB:GFP)* by FACS
271 (Figure 6a, Figure 6-figure supplement 1). Using RT-qPCR analysis of the GFP^{high} and
272 GFP^{low} populations, we then quantified the expression levels of selected candidate genes that
273 we previously found to be significantly enriched in beta-cells from older animals (1 ypf). We
274 found that *socs2* showed more than 2.5 fold higher expression (n=4 biological replicates, n=3
275 animals per replicate, 1000 cells per condition) in the GFP^{high} cells compared to GFP^{low},
276 whereas other genes did not exhibit significantly higher expression (Figure 6b, Figure 6-
277 source data 1).

278 To test if higher levels of *socs2* expression can inhibit beta-cell proliferation, we
279 generated a bi-cistronic construct containing CFP linked to *socs2* via a viral T2A sequence,
280 and placed it under the control of the insulin promoter. Injecting the plasmid in one-cell-stage
281 zebrafish embryos leads to mosaic and stochastic expression of *socs2* in beta-cells at later
282 stages (Figure 6c). To quantify the effect of *socs2* expression on proliferation, we injected the
283 plasmid in *Tg(ins:Fucci-G1);Tg(ins:Fucci-S/G2/M)* embryos, such that beta-cells in the
284 G0/G1 phases of cell-cycle were labelled in red, whereas cells in the S/G2/M phases of cell
285 cycle were labeled in green. The cells expressing *socs2* were also CFP-positive, allowing us
286 to distinguish them from wild-type beta-cells in the same islet (Figure 6d). We then
287 quantified the proportion of proliferating CFP-positive and CFP-negative beta-cells at 23-25
288 dpf, a stage characterized by higher rates of beta-cell proliferation. We found that whereas
289 8.44% ± 3.37 of the CFP-negative beta-cells were proliferating, only 1.08% ± 1.65 CFP-
290 positive beta-cells exhibited cell-cycle progression (n=9) (Figure 6e). Overexpression of CFP

291 alone, or CFP-T2A-*rapgef4* and CFP-T2A-*spry4* in this mosaic manner did not affect
292 proliferation (Figure 6-figure supplement 2). Thus, *socs2* can cell-autonomously inhibit beta-
293 cell proliferation. Altogether, these results suggest that the higher endogenous expression of
294 *socs2* in *NF-kB*:GFP^{high} compared to *NF-kB*:GFP^{low} beta-cells could contribute to the
295 proliferative heterogeneity among beta-cells based on the differences in NF-kB signaling
296 strength.
297
298
299
300 **Discussion**
301 Type 2 diabetes is an age-related disease, and hence, it is important to identify how
302 advancing age alters the islet. Our work shows that in zebrafish, NF-kB signaling becomes
303 preferentially active in beta-cells from older animals. An additional sign of islet inflammation
304 is the recruitment of intra-islet macrophages, a subset of which express the cytokine *tnfα*. In
305 addition, we show that beta-cells upregulate in a heterogeneous manner the TNFα receptor,
306 *tnfrsf1b*, and that *tnfα*-expression is sufficient to trigger NF-kB signaling activation.
307 Altogether, our results document the development of chronic islet inflammation in older
308 animals. Based on our data, we also propose that with age, beta-cell replication declines in a
309 heterogeneous manner, with high levels of NF-kB signaling marking the cells that lose
310 proliferative potential (Figure 7).
311 The relevance of our results extends beyond the zebrafish model, as they corroborate
312 empirical evidence gathered in human beta-cells. There is emerging evidence that chronic
313 inflammation is a characteristic of aging in human (Puchta *et al*, 2016) and is associated with
314 beta-cell dysfunction in type 2 diabetes (Nordmann *et al*, 2017). Moreover, the accumulation
315 of innate immune cells in islets in fish is reminiscent of changes observed in type 2 diabetes in
316 man (Nordmann *et al*, 2017). Furthermore, islets form older human donors exhibit an

317 increase in the number of intra-islet macrophages (Almaça *et al*, 2014), analogous to
318 zebrafish. Thus, our work puts forward the zebrafish as a new model to investigate the
319 mechanisms of beta-cell aging and the crosstalk between beta-cells and the innate immune
320 system, which is of relevance to understanding human disease.

321 Our work also adds to the burgeoning field of mammalian beta-cell heterogeneity. A
322 recent report from Bonner-Weir and colleagues (Aguayo-mazzucato *et al*, 2017) revealed
323 progressive increases in the proportion of beta cells expressing age-related markers, including
324 IGF-IR in older mice and human islets, suggesting that aging in mammalian beta-cells might
325 be a heterogeneous process. In our study, we identified a different marker of age-related
326 heterogeneity – NF-kB, and linked this to the proliferative decline of beta-cells, which is an
327 important age-related trait. Intriguingly, the human receptor *TNFRSF11A* (Receptor
328 Activator of NF-kB) shows markedly heterogeneous expression in adult human beta-cells
329 according to the single-cell sequencing database provided by the Sandberg lab
330 (http://sandberg.cmb.ki.se/pancreas/) (Segerstolpe *et al*, 2016). The significance of this
331 observation for human beta-cell heterogeneity needs further investigation. Notably,
332 TNFRSF11A antagonism can increase human beta-cell proliferation, implicating NF-kB
333 signaling in beta-cell proliferation (Kondegowda *et al*, 2015). Indeed, we found that in
334 zebrafish, beta-cells with higher levels of NF-kB signaling elevate *socs2* expression, which in
335 turn can reduce proliferation. Of note, adenovirus transduction of the functionally related
336 gene *socs3* in rat islets inhibits beta-cell proliferation (Lindberg *et al*, 2005). It will be
337 necessary to address whether NF-kB activates *socs2* directly or indirectly to control
338 proliferation.

339 Recent studies have proposed that beta-cell proliferation and functional maturity
340 exhibit an inverse correlation. For example, gene-expression analysis revealed that
341 proliferating beta-cells reduce the levels of transcripts required for beta-cell function
342 (Klochendler *et al*, 2016). In addition, lineage tracing of immature and mature beta-cells

343 within the same islet revealed higher proliferation of immature beta-cells (Singh *et al*, 2017).
344 In this regard, it will be important to explore whether beta-cells with higher NF-kB signaling
345 are functionally more mature compared to the ones with lower activity, and whether beta-cell
346 function increases in older zebrafish. To start addressing these questions, we performed
347 analysis of beta-cell functional connectivity of our calcium recordings using algorithms
348 developed in the Hodson and Rutter groups (Hodson *et al*, 2012, Johnston *et al*, 2016).
349 However, this analysis did not reveal conclusive changes in beta-cell connectivity with aging
350 (data not shown). In the future, it will be informative to develop new calcium fluorescent
351 reporters allowing to monitor and compare glucose-responsiveness of *NF-kB*:GFP^{low} and *NF-*
352 *kB*:GFP^{high} cells within the same islet.
353 An intriguing observation of our study is the presence of *tnfα*-positive macrophages in
354 the islets under basal conditions, which might indicate that these macrophages are activated
355 and pro-inflammatory (Nguyen-Chi *et al*, 2015). Under steady state, activated macrophages
356 are typically observed only in barrier organs, such as the lung and the intestine (Ferris *et al*,
357 2017). Our results now show that activated macrophages are also present in the islets of adult
358 zebrafish under physiological conditions. In agreement with our findings, a recent report
359 documented the presence of islet-resident macrophages expressing TNFα, IL1b and MHC-II
360 (Ferris *et al*, 2017) in non-obese diabetic (NOD) mice. However, despite the presence of
361 cytokine expression in the macrophages, Ferris et al. could not detect nuclear RelA (a member
362 of the NF-kB heterodimer) signaling in the islets, suggesting that beta-cells did not activate
363 NF-kB signaling. This might be a result of the lower sensitivity of their detection
364 method. Indeed, using a sensitive readout of NF-kB signaling based on a transgenic reporter,
365 we show that *tnfα*-expression alone is capable of inducing NF-kB activation in beta-cells.
366 However, we note that further studies and new tools will be necessary to address the crosstalk
367 between the innate immune cells and beta-cell inflammation. Furthermore, additional
368 inflammatory signals can originate from cells other than the macrophages. For example,

369 acinar cells were recently shown to express TNFα, which in turn induces apoptosis in aged
370 mouse beta-cells (Xiong *et al*, 2017).
371 Besides paracrine factors, NF-kB activity might be regulated by beta-cell intrinsic
372 factors. In particular, ER stress is known to activate NF-kB signaling in multiple cell types
373 (Tam *et al*, 2012). It is possible that with aging, beta-cells experience higher levels of ER
374 stress and thereby activate NF-kB signaling. Therefore, a good question for the future will be
375 to define the contribution of extrinsic and intrinsic factors, including ER-stress, to the
376 heterogeneous activation of inflammation in beta-cells. Our study opens the possibility to use
377 *Danio rerio* as a new model for gaining insights into the links between aging and beta-cell
378 biology and the relationship between the innate immune system and diabetes.
379
380
381
382
383
384
385
386
387
388
389
390
391
392
393
394

395

396 **Materials and methods**

397 **Key Resources Table**

Reagent type (species) or resource	Designation	Source or reference	Identifiers	Additional information
gene (*Danio rerio*)	*flag-tnfrsf1b*	synthesized from GenScript		
gene (*Danio rerio*)	*tnfα*	Dharmacon	MDR1734-202796946	ZGC tnfa cDNA (CloneId:8148192)
gene (*Danio rerio*)	*cpf-T2A*	synthesized from GenScript		
genetic reagent (*Danio rerio*)	*Tg(ins:FUCCI-G1)^{s948}*	PMID: 23791726		
genetic reagent (*Danio rerio*)	*Tg(ins:FUCCI-S/G2/M)^{s946}*	PMID: 23791726		
genetic reagent (*Danio rerio*)	*Tg(NF-kB:GFP)*	PMID: 21439961		
genetic reagent (*Danio rerio*)	*TgBAC(tnfa:GFP)*	PMID: 25730872		
genetic reagent (*Danio rerio*)	*Tg(ins:nlsRenilla-mKO2)*	PMID: 28939870		
genetic reagent (*Danio rerio*)	*Tg(ins:BB1.0L)*	PMID: 28939870		
genetic reagent (*Danio rerio*)	*Tg(ins:gCaMP6s; cryaa:mCherry)*	PMID: 28939870		
genetic reagent (*Danio rerio*)	*Tg(ins: loxP:mCherrySTOP:loxP:H2B-GFP)*	PMID: 21497092		
genetic reagent (*Danio rerio*)	*Tg(mpeg1:mCherry)*	PMID: 21084707		
antibody	anti-insulin	Dako	A0564	guinea pig (1:200)
antibody	anti-EGFP	Abcam	ab13970	chicken (1:500)
antibody	anti-PCNA	Dako	M0879	mouse (1:500)
antibody	anti-L-plastin	Biozol	LS-C210139-250	rabbit (1:1000)
antibody	Alexa Fluor488, 568 and 647 secondaries	Molecular Probes		(1:300)
recombinant DNA reagent	*ins:Flag-tnfrsf1b;cryaa:RFP* (plasmid)	This paper		cloned into *ins:MCS2;cryaa:RFP*
recombinant DNA reagent	*ins:tnfα;cryaa:CFP* (plasmid)	This paper		cloned by replacing *mCherry-zCdt1* with *tnfα* in *ins:mCherry-zCdt1;cryaa:CFP*
recombinant DNA reagent	*ins:CFP-T2A-socs2;cryaa:RFP* (plasmid)	This paper		cloned into *ins:MCS2;cryaa:RFP*
recombinant DNA reagent	*ins:CFP-T2A-rapgef4;cryaa:RFP* (plasmid)	This paper		cloned into *ins:MCS2;cryaa:RFP*

recombinant DNA reagent	*ins:CFP-T2A-spry4;cryaa:RFP* (plasmid)	This paper		cloned into *ins:MCS2;cryaa:RFP*
recombinant DNA reagent	*ins:mAG-zGeminin;cryaa:RFP* (plasmid)	PMID: 23791726		
recombinant DNA reagent	*ins:MCS2;cryaa:RFP* (plasmid)	PMID: 28939870		
recombinant DNA reagent	*ins:mCherry-zCdt1;cryaa:CFP* (plasmid)	PMID: 23791726		
software, algorithm	edgeR package	PMID:19910308		
other	TSQ (N-(6-Methoxy-8-Quinolyl)-p-Toluenesulfonamide)	ThermoFisher	M-688	30 µM

398

399 **Zebrafish strains and husbandry**

400 Wild-type or transgenic zebrafish of the outbred TL, AB, WIK strains were used in all
401 experiments. Zebrafish were raised under standard conditions at 28°C. Animals were chosen
402 at random for all experiments. Published transgenic strains used in this study were
403 *Tg(ins:FUCCI-G1)*^{s948} (Ninov *et al*, 2013), *Tg(ins:FUCCI-S/G2/M)*^{s946} (Ninov *et al*, 2013),
404 *Tg(NF-kB:GFP)* (Kanther *et al*, 2011), *TgBAC(tnfa:GFP)* (Marjoram *et al*, 2015),
405 *Tg(ins:nlsRenilla-mKO2)* (Singh *et al*, 2017), *Tg(ins:BB1.0L)* (Singh *et al*, 2017), *Tg(ins:*
406 *loxP:mCherrySTOP:loxP:H2B-GFP)* abbreviated as *Tg(ins:mCherry)* (Hesselson *et al*,
407 2011), *Tg(mpeg1:mCherry)* (Ellett *et al*, 2011). Experiments were conducted in accordance
408 with the Animal Welfare Act and with permission of the Landesdirektion Sachsen, Germany
409 (AZ 24–9168, TV38/2015, A12/2016, A5/2017).

410 **Cloning and constructs**

411 To generate *ins:Flag-tnfrsf1b;cryaa:RFP*, a vector was created by inserting multiple
412 cloning sites (MCS2) downstream of the insulin promoter to yield *ins:MCS2;cryaa:RFP*. To
413 do so, the plasmid *ins:mAG-zGeminin;cryaa:RFP* was digested with EcoRI/PacI and ligated
414 with dsDNA generated by annealing two primers harboring the sites SpeI, BamHI, EcoRV
415 and flanked by EcoRI/PacI overhangs. The plasmid pUC consisting of the *tnfrsf1b* flanked by

416 EcoRI/PacI sites was synthesized from GenScript. Primers were designed such that EcoRI
417 site was destroyed in the process of inserting *tnfrsf1b* under the insulin promoter.
418 *ins:MCS2;cryaa:RFP* and the plasmid *pUC-Flag-tnfrsf1b* were subsequently digested with
419 EcoRI/PacI to yield compatible fragments, which were ligated together to yield the final
420 construct. The entire construct was flanked with I-SceI sites to facilitate transgenesis.
421 To generate *ins:CFP-T2A-socs2;cryaa:RFP*, a vector was created by inserting
422 multiple cloning sites (MCS2) downstream of the insulin promoter to yield *ins:MCS2;*
423 *cryaa:RFP*. To do so, the plasmid *ins:mAG-zGeminin;cryaa:RFP* was digested with
424 EcoRI/PacI and ligated with dsDNA generated by annealing two primers harboring the sites
425 SpeI, BamHI, EcoRV and flanked by EcoRI/PacI overhangs. The plasmid pUC consisting of
426 the candidate gene *socs2* fused to CFP via T2A sequence flanked by EcoRI/PacI sites was
427 synthesized from GenScript. Primers were designed such that the EcoRI site was destroyed in
428 the process. *ins:MCS2;cryaa:RFP* and the plasmid *pUC-CFP-T2A-socs2* were subsequently
429 digested with EcoRI/PacI to yield compatible fragments, which were ligated together to yield
430 the final construct. The entire construct was flanked with I-SceI sites to facilitate
431 transgenesis. Same process as described above was used for generating *ins:CFP-T2A-*
432 *spry4;cryaa:RFP* construct.
433 To generate *ins:CFP-T2A-rapgef4;cryaa:RFP*, a plasmid pUC consisting of rapgef4
434 flanked by SpeI/PacI sites was synthesized from GenScript. *ins:CFP-T2A-socs2;cryaa:RFP*
435 and the plasmid *pUC-rapgef4* were subsequently digested with SpeI/PacI to yield compatible
436 fragments, which were ligated together to yield the final construct.
437 **Analysis of proliferation using mosaic integration in the genome**
438 For counting beta-cells in *Tg(ins:FUCCI-G1);Tg(ins:FUCCI-S/G2/M)* with mosaic
439 expression of candidate genes, the "spots" function of Imaris (Bitplane) was used after
440 thresholding. The total number of CFP-positive red cells and CFP-negative red cells in the

441 entire islet spanning all stacks were calculated. All the *Tg(ins:FUCCI-S/G2/M)*-positive cells

442 were counted manually for CFP-positive and CFP-negative beta-cells.

$$\text{Percentage of CFP-positive proliferating cells} = \frac{(\text{CFP-positive}) + (\text{ins:Fucci-S/G2/M-positive and ins:FUCCI-G1-negative cells})}{(\text{Total CFP-positive cells})} \times 100$$

443

$$\text{Percentage of CFP-negative proliferating cells} = \frac{(\text{CFP-negative}) + (\text{ins:Fucci-S/G2/M-positive and ins:FUCCI-G1-negative cells})}{(\text{Total CFP-negative cells})} \times 100$$

444 **Tissue collection and sectioning**

445 To facilitate confocal imaging of the islet, the pancreas was dissected from the gut

446 (juvenile and adults) after fixation. Fish were euthanized in Tricaine prior to dissection of

447 gut, and the samples immersed in 4% paraformaldehyde for 48 hours at 4°C. The pancreas

448 was then manually dissected and washed multiple times in PBS.

449 For cryo-sectioning, the tissue was then immersed in 20% sucrose solution overnight

450 at 4°C. The tissue was then embedded in 20% sucrose + 7.5% gelatin solution in cryo-molds

451 on dry ice and sectioned at 14 μm in thickness with Leica cryostat.

452 **Cell counting**

453 Total number of beta-cells in the islets were counted using Imaris (Bitplane). For

454 counting beta-cells in *Tg(ins:FUCCI-G1);Tg(ins:FUCCI-S/G2/M)*, the "spots" function of

455 Imaris, with appropriate thresholding, was used to count all the red cells in stacks spanning

456 the entire islet. All the proliferating cells (green only) were counted manually. This approach

457 enabled us to quantify the percentage of proliferating beta-cells in the whole islet.

$$\text{Percentage of proliferating cells} = \frac{(\text{ins:Fucci-S/G2/M-positive and ins:FUCCI-G1-negative cells})}{\text{Total beta-cells}} \times 100$$

458

459

460 **EdU labeling**

461 To label proliferating cells, 3 mpf fish were placed in 2 mM EdU on two consecutive
462 nights, and then placed back in system water with normal feeding during each day. The fish
463 were then euthanized, the gut was fixed and the pancreas was sectioned as described above.
464 The tissue sections were washed 3 X 10 min with PBS, and EdU detection was performed
465 according to the kit protocol Click- iT® EdU Alexa Fluor® 647 Imaging Kit (C10340 Fisher
466 Scientific). GFP and insulin staining was performed at the concentrations described below.

467 **Immunofluorescence and image acquisition**

468 Immunofluorescence was performed on pancreas sections prepared as described
469 above. Antigen retrieval was carried out prior to anti-PCNA staining by treating the sections
470 with 10 mM citrate buffer (pH=6) for 10 mins at 90°C. The sections were permeabilized in
471 1% PBT (TritonX-100) and blocked in 4% PBTB (BSA). Primary and secondary antibody
472 staining was performed overnight at 4°C. Primary antibodies used in this study were anti-
473 insulin (guinea pig, Dako A0564) at 1:200, anti-EGFP (chicken, abcam ab13970) at 1:500,
474 anti-PCNA (mouse, Dako, M0879) at 1:500, and anti-L-plastin (rabbit, Biozol LS-C210139-
475 250) at 1:1000. Secondary antibodies used in this study were Alexa Fluor 568 and Alexa
476 Fluor 488 anti-guinea pig (1:300), Alexa Fluor 647 anti-rabbit and anti-mouse (1:300) and
477 Alexa Fluor 488 anti-chicken (1:300). Samples were mounted in Vectashield and imaged
478 using a Zeiss LSM 780.

479 **GCAMP6s image acquisition and analysis**

480 To monitor the changes in glucose-stimulated calcium influx during development, GCAMP6s
481 measurements were performed on isolated islets from *Tg(ins:gCaMP6s;*
482 *cryaa:mCherry);Tg(ins:Renilla-mKO2; cryaa:CFP)* double-transgenic animals at 3 mpf.
483 Freshly dissected islets from euthanized fish were washed with HBSS containing Ca2+/Mg2+
484 (Life technologies, 14175095) twice and embedded in fibrin gels (3:1 ratio of 10 mg/ml
485 Bovine fibrinogen, 50 U/ml Bovine thrombin; Sigma Aldrich). Upon polymerization, islets

486 were immersed in HBSS containing 5 mM glucose, visually oriented along A/P axis and
487 imaged using live confocal microscopy (LSM-780 FLIM inverse) to establish the baseline.

488 **Fluorescent intensity analysis**

489 Normalized GFP fluorescent intensity of insulin-positive cells on pancreatic islet
490 sections was measured using Fiji (Schindelin *et al*, 2012). An insulin-positive cell was first
491 located by going through individual sections in the confocal z-stack. The optical section
492 containing the largest area of the nucleus was chosen as the center of the cell. A region-of-
493 interest (ROI) was drawn around the nucleus and the fluorescence intensity of the GFP and
494 DAPI channels were recorded. The normalized GFP intensity was calculated as a ratio of
495 mean GFP intensity and mean DAPI intensity for each ROI. For EdU or PCNA intensity
496 measurements, mean grey intensity value for the EdU or PCNA channel was calculated along
497 with the GFP and DAPI channels in each ROI created at the center of a cell, as described
498 above. To discriminate between GFP^{high} and GFP^{low} cells, a threshold was set for each islet
499 individually. The threshold (GFP^{total}) was calculated as the average normalized GFP intensity
500 of all the images belonging to one islet. Threshold for determining EdU or PCNA positive
501 cells was set by eye.

502 The GFP fluorescence intensity of the secondary islets in *Tg(NF-kB:GFP)* animals
503 was calculated with the Imaris software by using the surface function. Surfaces were
504 rendered for each secondary islet using the same threshold. The mean GFP fluorescence
505 intensity and volume within these surfaces was recorded. The GFP fluorescence was
506 normalized to the volume of the secondary islets.

507 **Cell Culture of sorted beta-cells**

508 Beta-cells were dissociated from 3 mpf *Tg(NF-kB:GFP);Tg(ins:mCherry)* islets and
509 FAC-sorted as described above. The single beta-cells were sorted into a 384-well plate,
510 containing the final cell-culture media (50% L-15 (Gibco, 11415-049), 50% DMEM (Gibco,
511 31966-021), 10% FBS (Gibco, 10500-064) and 1x antibiotics (Sigma, A5955)). The plates

512 were incubated in a cell-culture incubator at 27 °C with 5% CO_2. Individual beta-cells were
513 imaged using Zeiss LSM-780 inverse confocal microscope. The GFP fluorescence intensity
514 was measured using the ROI function of Fiji as described above.

515 **FACS and gene profile analysis**

516 For RNA-Seq, RT-qPCR and NF-kB population analysis, beta-cell isolated from islets
517 were sorted and analyzed using FACS-Aria II (BD Bioscience). For dissociation, islets were
518 collected in PBS chilled on ice. After one washing with ice cold PBS, islets were dissociated
519 into single cells by incubation in TrypLE (ThermoFisher, 12563029) with 0.1% Pluronic F-68
520 (ThermoFisher, 24040032) at 37 °C in a benchtop shaker set at 350 rpm for 50 min.
521 Following dissociation, TrypLE was inactivated with 10% FBS, and the cells pelleted by
522 centrifugation at 500g for 10 min at 4 °C. The supernatant was carefully discarded and the
523 pellet re-suspended in 500 uL of HBSS (without Ca, Mg) + 0.1% Pluronic F-68. To remove
524 debris, the solution was passed over a 30 µm cell filter (Miltenyi Biotec, 130-041-407).

525 For RNA-Sequencing, total RNA was extracted from FACS sorted beta-cells using
526 Quick-RNA MicroPrep kit (R1050 Zymo Research). Sequencing was performed on llumina
527 HiSeq2500 in 2x75bp paired-end mode. Reads were splice-aligned to the zebrafish genome,
528 GRCz10, using GSNAP and known splice sites from Ensembl gene annotation, version 81.
529 FeatureCounts was used to assign reads to exons thus eventually getting counts per gene.
530 EdgeR package of R (Robinson *et al*, 2009) was used to perform differential analysis between
531 samples. Across-samples normalization was performed using the TMM normalization
532 method.

533 For single-cell RT-qPCR, cDNA was synthesized with Quanta qScript TM cDNA
534 Supermix directly on cells. Total cDNA was pre-amplified for 16 cycles (1x 95ºC 8', 18x
535 (95ºC 45'', 49ºC* 1.30', 72ºC 1.5') 1x 72ºC 7') (* with 0.3ºC increment/cycle) with the
536 QIAGEN Multiplex PCR Plus Kit (Qiagen) in a final volume of 35 µl in the presence of the
537 10 primer pairs (listed in Table S1) (25nM final for each primer). Pre-amplified DNA (10 µl)

538 was treated with 1.2 U Exonuclease I and expression quantified by real time PCR on the
539 BioMark™ HD System (© Fluidigm Corporation, CA, USA) using the 96.96 Dynamic Array
540 IFC and the GE 96x96 Fast PCR+ Melt protocol and SsoFast EvaGreen Supermix with Low
541 ROX (BIO RAD, CA, USA) with 5 µM primers (described above) for each assay. Raw data
542 was analyzed using the Fluidigm Real-Time PCR analysis software.

543 For bulk RT-qPCR gene expression profiling, 1000 GFP^{high} and GFP^{low} cells were
544 sorted into 5 µl EB Buffer (Qiagen) containing 0.3% IGEPAL and 0.1% BSA and
545 immediately snap frozen. The cells were then thawed and incubated on ice for 10'. cDNA was
546 synthesized with Quanta qScript TM cDNA Supermix directly on cells in a final volume of 30
547 µl. 15 µl. of cDNA was pre-amplified for 12 cycles (1x 95ºC 1', 95ºC 15'', 60ºC 1', 72ºC
548 1.5') and 1x 72ºC 10' with the TATAA GrandMaster Mix (TATAA Biocenter, Göteborg,
549 Sweden) in a final volume of 35 µl in the presence of primer pairs for the following genes:
550 ins, cish, spry4, trib3, rapgef4, ef1a, bact2, rpl13, tnfa, tnfrsf1b, socs23 (25nM final for each
551 primer). 1.2 µl pre-amplified cDNA was used for quantification by real time PCR on the
552 LightCycler480 (Roche, Switzerland) using SYBR® Premix Ex Taq TM (Tli RNaseH Plus)
553 (Takara BIO USA, INC.) and 0.2 nM of each primer in a volume of 10 µl using the following
554 cycling program: initial denaturation 95ºC 30'', amplification 45x (95ºC 5'', 60ºC 30'') and
555 melting curves 1x (95ºC 5'', 60ºC 1', ramp to 95ºC (ramping rate 0.11)) followed by 30''
556 cooling at 50ºC. Raw data was analyzed using the LightCycler480 analysis software.

557 For analysis the levels of *NF-kB*:GFP by FACS, dissociated cells were incubated in 30
558 µM solution of TSQ (N-(6-Methoxy-8-Quinolyl)-p-Toluenesulfonamide) (ThermoFisher, M-
559 688) for 20 mins to label beta-cells. The cells were pelleted by centrifugation at 500g for 10
560 min at 4 °C. The supernatant was carefully discarded and the pellet re-suspended in 500 µL of
561 HBSS (without Ca, Mg) + 0.1% Pluronic F-68. To remove debris, the solution was passed
562 over a 30 µm cell filter (Miltenyi Biotec, 130-041-407) and proportion of *NF-kB:*GFP^{high} and
563 *NF-kB:*GFP^{low} cells were analyzed by FACS.

564 For correlation analysis of GFP fluorescence intensity with GFP mRNA, beta-cells
565 from 3 mpf *Tg(ins:mCherry);Tg(NF-kB:GFP)* animals were dissociated as described above.
566 Single beta-cells were sorted into 96-well plates using the index sort function of Aria II. This
567 allowed us to record the GFP fluorescence intensity of each sorted beta-cell. Single-cell RT-
568 qPCR was performed on the FAC-sorted cells for *GFP* and *b-actin1* mRNA as described
569 above.

570 **Analysis of single-cell RT-qPCR data**

571 Single cell RT-qPCR data was obtained from Fluidigm as Ct values of gene
572 expression per cell. The Fluidigm assay performs 40 cycles of amplification. If the
573 fluorescence signal from RT-qPCR does not cross threshold after 40 cycles, then the gene is
574 considered to be "not detected", and set as Ct=40 (McDavid *et al*, 2013). A gene was
575 classified as "detected" for the value of Ct<40 in a given cell (McDavid *et al*, 2013). Pre-
576 analysis cleanup of the RT-qPCR data was performed by removing cells with undetected
577 values (Ct = 40) for the house keeping genes *b-actin1*, *ef1α* or *rpl13α*. For the beta-cells from
578 3 mpf and 1 ypf animals, the proportion of cells with detectable candidate gene expression
579 was calculated as:

$$\text{Percentage of cells expressing a candidate gene} = \frac{\text{cells with Ct<40 for the candidate gene}}{\text{Total cells}} \times 100$$

580

581 Significance testing for differences in proportion of cells with detectable gene expression was
582 performed using Pearson's Chi-Square test. The Ct values were $-\log_{10}$ transformed for
583 representation purpose, such that $-\log_{10}(40) \sim -1.6$ is considered undetectable gene expression
584 level.

585 **Statistical analysis**

586 No statistical methods were used to predetermine sample size. The experiments were not
587 blinded. Graphs were plotted using R. Statistical analysis was performed using R and

588 Microsoft Excel. Values were compared using unpaired Students t-test or ANOVA as
589 indicated for each experiment. P-values of <0.05 were considered statistically significant.
590 Data are expressed as mean ± standard deviation (SD) unless otherwise specified.

591 **Source data:**

592 The raw files and raw count table from deep sequencing can be accessed at GEO with
593 accession number GSE106938 (with Token number qpybiywarhwpnyd).

594 **Acknowledgments:**

595 We thank Max Yun, and members of the Ninov lab for comments on the manuscript,
596 members of CRTD fish, microscopy and FACS facilities for technical assistance. We thank
597 John Rawls for *Tg(NF-kB:GFP)* reporter line and Michel Bagnat for *TgBAC(tnfα:GFP)*
598 reporter line. D.J.H. was supported by a Diabetes UK R.D. Lawrence (12/0004431) and
599 EFSD/Novo Nordisk Rising Star Fellowships, a Wellcome Trust Institutional Support Award,
600 and an MRC Project Grant (MR/N00275X/1). G.A.R. was supported by Wellcome Trust
601 Senior Investigator (WT098424AIA) and Royal Society Wolfson Research Merit Awards,
602 and by MRC Programme (MR/J0003042/1), MRC Project (MR/N00275X/1), Biological and
603 Biotechnology Research Council (BB/J015873/1) and Diabetes UK Project (11/0004210)
604 grants. This project has received funding from the European Research Council (ERC) under
605 the European Union's Horizon 2020 research and innovation programme (Starting Grant
606 715884 to D.J.H.). N.N. is supported by funding from the DFG–Center for Regenerative
607 Therapies Dresden, Cluster of Excellence at TU Dresden and the German Center for Diabetes
608 Research (DZD), as well as research grants from the German Research Foundation (DFG), the
609 European Foundation for the Study of Diabetes (EFSD) and the DZD.

610

611

612

613

614 **References**

615 Aguayo-mazzucato C, Haaren M Van, Mruk M, Jr. TBL, Crawford C, Hollister-Lock J,
616 Sullivan BA, Johnson JW, Ebrahimi A, Dreyfuss JM, Deursen J Van, Weir GC &
617 Bonner-weir S (2017) b Cell Aging Markers Have Heterogeneous Distribution and Are
618 Induced by Insulin Resistance. *Cell Metab.* **25:** 898–910.e5 Available at:
619 http://dx.doi.org/10.1016/j.cmet.2017.03.015

620 Almaça J, Molina J, Arrojo E Drigo R, Abdulreda MH, Jeon WB, Berggren P-O, Caicedo A
621 & Nam HG (2014) Young capillary vessels rejuvenate aged pancreatic islets. *Proc. Natl.*
622 *Acad. Sci. U. S. A.* **111:** 17612–7 Available at:
623 http://www.ncbi.nlm.nih.gov/pubmed/25404292

624 Arda HE, Li L, Tsai J, Powers AC, Chang HY, Kim SK, Arda HE, Li L, Tsai J, Torre EA,
625 Rosli Y, Peiris H & Spitale RC (2016) Age-Dependent Pancreatic Gene Regulation
626 Reveals Mechanisms Governing Human b Cell Function-supp. *Cell Metab.* **23:** 1–12
627 Available at: http://dx.doi.org/10.1016/j.cmet.2016.04.002

628 Avrahami D, Li C, Zhang J, Schug J, Avrahami R, Rao S, Stadler MB, Burger L, Schübeler
629 D, Glaser B & Kaestner KH (2015) Aging-Dependent Demethylation of Regulatory
630 Elements Correlates with Chromatin State and Improved β Cell Function. *Cell Metab.*
631 **22:** 619–632 Available at:
632 http://linkinghub.elsevier.com/retrieve/pii/S1550413115003885

633 Bader E, Migliorini A, Gegg M, Moruzzi N, Gerdes J, Roscioni SS, Bakhti M, Brandl E,
634 Irmler M, Beckers J, Aichler M, Feuchtinger A, Leitzinger C, Zischka H, Wang-Sattler
635 R, Jastroch M, Tschöp M, Machicao F, Staiger H, Häring H-U, et al (2016) Identification
636 of proliferative and mature β-cells in the islets of Langerhans. *Nature* **535:** 430–434
637 Available at:
638 http://www.nature.com/doifinder/10.1038/nature18624%5Cnhttp://www.ncbi.nlm.nih.go
639 v/pubmed/27398620

640 Carboneau BA, Allan JA, Townsend SE, Kimple ME, Breyer RM & Gannon M (2017)
641 Opposing effects of prostaglandin E2 receptors EP3 and EP4 on mouse and human β-cell
642 survival and proliferation. *Mol. Metab.* **6:** 548–559 Available at:
643 http://dx.doi.org/10.1016/j.molmet.2017.04.002
644 Dorrell C, Schug J, Canaday PS, Russ HA, Tarlow BD, Grompe MT, Horton T, Hebrok M,
645 Streeter PR, Kaestner KH & Grompe M (2016) Human islets contain four distinct
646 subtypes of [beta] cells. *Nat. Commun.* **7:** 1–9 Available at:
647 http://dx.doi.org/10.1038/ncomms11756
648 Ellett F, Pase L, Hayman JW, Andrianopoulos A & Lieschke GJ (2011) Mpeg1 Promoter
649 Transgenes Direct Macrophage-Lineage Expression in Zebrafish. *Blood* **117:** e49-56
650 Espı´n-Palazo´n R, Stachura DL, Campbell CA, Garcı D, Cid N Del, Mulero V, Traver D,
651 Kim AD & Candel S (2014) Proinflammatory Signaling Regulates Hematopoietic Stem
652 Cell Emergence. *Cell 159, 1070–1085*
653 Fang N, Zhang W, Xu S, Lin H, Wang Z, Liu H, Fang Q, Li C, Peng L & Lou J (2014)
654 TRIB3 alters endoplasmic reticulum stress-induced β-cell apoptosis via the NF-κB
655 pathway. *Metabolism.* **63:** 822–830 Available at:
656 http://dx.doi.org/10.1016/j.metabol.2014.03.003
657 Ferris ST, Zakharov PN, Wan X, Calderon B, Artyomov MN, Unanue ER & Carrero JA
658 (2017) The islet-resident macrophage is in an inflammatory state and senses microbial
659 products in blood The Journal of Experimental Medicine. *J. Exp. Med* **214:** 2369–2385
660 Hesselson D, Anderson RM & Stainier DYR (2011) Suppression of Ptf1a activity induces
661 acinar-to-endocrine conversion. *Curr. Biol.* **21:** 712–717 Available at:
662 http://dx.doi.org/10.1016/j.cub.2011.03.041
663 Hodson DJ, Romanò N, Schaeffer M, Fontanaud P, Lafont C, Fiordelisio T & Mollard P
664 (2012) Coordination of calcium signals by pituitary endocrine cells in situ. *Cell Calcium*
665 **51:** 222–230 Available at: http://dx.doi.org/10.1016/j.ceca.2011.11.007

666 Huang DW, Lempicki RA & Sherman BT (2009a) Systematic and integrative analysis of
667 large gene lists using DAVID bioinformatics resources. *Nat. Protoc.* **4:** 44–57
668 Huang DW, Sherman BT & Lempicki RA (2009b) Bioinformatics enrichment tools: Paths
669 toward the comprehensive functional analysis of large gene lists. *Nucleic Acids Res.* **37:**
670 1–13
671 Kanther M, Sun X, Mühlbauer M, Mackey LC, Flynn EJ, Bagnat M, Jobin C & Rawls JF
672 (2011) Microbial colonization induces dynamic temporal and spatial patterns of NF-kB
673 activation in the zebrafish digestive tract. *Gastroenterology* **141:** 197–207 Available at:
674 http://dx.doi.org/10.1053/j.gastro.2011.03.042
675 Kato H, Nomura K, Osabe D, Shinohara S, Mizumori O, Katashima R, Iwasaki S, Nishimura
676 K, Yoshino M, Kobori M, Ichiishi E, Nakamura N, Yoshikawa T, Tanahashi T,
677 Keshavarz P, Kunika K, Moritani M, Kudo E, Tsugawa K, Takata Y, et al (2006)
678 Association of single-nucleotide polymorphisms in the suppressor of cytokine signaling
679 2 (SOCS2) gene with type 2 diabetes in the Japanese. *Genomics* **87:** 446–458
680 Kim BJ, Kim YH, Kim S, Kim JW, Koh JY, Oh SH, Lee MK, Kim KW & Lee MS (2000)
681 Zinc as a paracrine effector in pancreatic islet cell death. *Diabetes* **49:** 367–372
682 Klochendler A, Caspi I, Corem N, Moran M, Friedlich O, Elgavish S, Nevo Y, Helman A,
683 Glaser B, Eden A, Itzkovitz S & Dor Y (2016) The genetic program of pancreatic β-cell
684 replication in vivo. *Diabetes* **65:** 2081–2093
685 Kondegowda NG, Fenutria R, Pollack IR, Orthofer M, Garcia-Ocan A, Penninger JM &
686 Vasavada RC (2015) Osteoprotegerin and Denosumab Stimulate Human Beta Cell
687 Proliferation through Inhibition of the Receptor Activator of NF- k B Ligand Pathway.
688 *Cell Metab.* **22:** 77–85
689 Lebrun P, Cognard E, Gontard P, Bellon-Paul R, Filloux C, Berthault MF, Magnan C,
690 Ruberte J, Luppo M, Pujol A, Pachera N, Herchuelz A, Bosch F & Van Obberghen E
691 (2010) The suppressor of cytokine signalling 2 (SOCS2) is a key repressor of insulin

692 secretion. *Diabetologia* **53:** 1935–1946

693 Lindberg K, Rønn SG, Tornehave D, Richter H, Hansen JA, Rømer J, Jackerott M &
694 Billestrup N (2005) Regulation of pancreatic β-cell mass and proliferation by SOCS-3. *J.*
695 *Mol. Endocrinol.* **35:** 231–243

696 Liu L, Brown D, McKee M, LeBrasseur NK, Yang D, Albrecht KH, Ravid K & Pilch PF
697 (2008) Deletion of Cavin/PTRF Causes Global Loss of Caveolae, Dyslipidemia, and
698 Glucose Intolerance. *Cell Metab.* **8:** 310–317

699 Marjoram L, Alvers A, Deerhake ME, Bagwell J, Mankiewicz J, Cocchiaro JL, Beerman RW,
700 Willer J, Sumigray KD, Katsanis N, Tobin DM, Rawls JF, Goll MG & Bagnat M (2015)
701 Epigenetic control of intestinal barrier function and inflammation in zebrafish. *Proc.*
702 *Natl. Acad. Sci. U. S. A.* **112:** 2770–5 Available at:
703 http://www.pnas.org/content/112/9/2770.long#sec-3

704 Mathias JR, Dodd ME, Walters KB, Yoo SK, Erik A & Huttenlocher A (2010)
705 Characterization of Zebrafish Larval Inflammatory Macrophages. *Dev Comp Immunol.*
706 **33:** 1212–1217

707 McDavid A, Finak G, Chattopadyay PK, Dominguez M, Lamoreaux L, Ma SS, Roederer M
708 & Gottardo R (2013) Data exploration, quality control and testing in single-cell qPCR-
709 based gene expression experiments. *Bioinformatics* **29:** 461–467

710 Meulen T Van Der, Mawla AM, Digruccio MR, Adams MW, Nies V, Lleman SD, Liu S,
711 Ackermann AM, Ceres EC, Hunter AE, Kaestner KH, Donaldson CJ & Huising MO
712 (2017) Virgin Beta Cells Persist throughout Life at a Neogenic Niche within Pancreatic
713 Islets. *Cell Metab.* **25:** 911–926

714 Nair AK, Muller YL, McLean NA, Abdussamad M, Piaggi P, Kobes S, Weil EJ, Curtis JM,
715 Nelson RG, Knowler WC, Hanson RL & Baier LJ (2014) Variants associated with type 2
716 diabetes identified by the transethnic meta-analysis study: assessment in American
717 Indians and evidence for a new signal in LPP. *Diabetologia* **57:** 2334–2338

718 Nguyen-Chi M, Laplace-Builhe B, Travnickova J, Luz-Crawford P, Tejedor G, Phan QT,
719 Duroux-Richard I, Levraud JP, Kissa K, Lutfalla G, Jorgensen C & Djouad F (2015)
720 Identification of polarized macrophage subsets in zebrafish. *Elife* **4:** 1–14
721 Ninov N, Hesselson D, Gut P, Zhou A, Fidelin K & Stainier DYR (2013) Metabolic
722 regulation of cellular plasticity in the pancreas. *Curr. Biol.* **23:** 1242–1250 Available at:
723 http://dx.doi.org/10.1016/j.cub.2013.05.037
724 Nordmann TM, Dror E, Schulze F, Traub S, Berishvili E, Barbieux C, Böni-Schnetzler M &
725 Donath MY (2017) The Role of Inflammation in β-cell Dedifferentiation. *Sci. Rep.* **7:** 1–
726 10
727 Parsons A, T C Brelje & Sorenson L (1992) Adaptation of islets of Langerhans to pregnancy:
728 increased islet cell proliferation and insulin secretion correlates with the onset of
729 placental lactogen secretion. *Endocrinol. 1992 Mar;130(3)1459-66*
730 Perl SY, Kushner JA, Buchholz BA, Meeker AK, Stein GM, Hsieh M, Kirby M, Pechhold S,
731 Liu EH, Harlan DM & Tisdale JF (2010) Significant human ??-cell turnover is limited to
732 the first three decades of life as determined by in vivo thymidine analog incorporation
733 and radiocarbon dating. *J. Clin. Endocrinol. Metab.* **95:** 234–239
734 Puchta A, Naidoo A, Verschoor CP, Loukov D, Thevaranjan N, Mandur TS, Nguyen PS,
735 Jordana M, Loeb M, Xing Z, Kobzik L, Larché MJ & Bowdish DME (2016) TNF Drives
736 Monocyte Dysfunction with Age and Results in Impaired Anti-pneumococcal Immunity.
737 *PLoS Pathog.* **12:** 1–23
738 Robinson MD, McCarthy DJ & Smyth GK (2009) edgeR: A Bioconductor package for
739 differential expression analysis of digital gene expression data. *Bioinformatics* **26:** 139–
740 140
741 Salpeter SJ, Khalaileh A, Weinberg-Corem N, Ziv O, Glaser B & Dor Y (2013) Systemic
742 regulation of the age-Related decline of pancreatic b-Cell replication. *Diabetes* **62:**
743 2843–2848

744 Schindelin J, Arganda-Carreras I, Frise E, Kaynig V, Longair M, Pietzsch T, Preibisch S,
745 Rueden C, Saalfeld S, Schmid B, Tinevez J-Y, White DJ, Hartenstein V, Eliceiri K,
746 Tomancak P & Cardona A (2012) Fiji: an open-source platform for biological-image
747 analysis. *Nat. Methods* **9:** 676–682 Available at:
748 http://www.nature.com/doifinder/10.1038/nmeth.2019
749 Segerstolpe Å, Palasantza A, Eliasson P, Andersson E-M, Andréasson A-C, Sun X, Picelli S,
750 Sabirsh A, Clausen M, Bjursell MK, Smith DM, Kasper M, Ämmälä C & Sandberg R
751 (2016) Single-Cell Transcriptome Profiling of Human Pancreatic Islets in Health and
752 Type 2 Diabetes. *Cell Metab.***:** 593–607 Available at:
753 http://linkinghub.elsevier.com/retrieve/pii/S1550413116304363
754 Singh SP, Janjuha S, Hartmann T, Kayisoglu Ö, Konantz J, Birke S, Murawala P, Alfar EA,
755 Murata K, Eugster A, Tsuji N, Morrissey ER, Brand M & Ninov N (2017) Different
756 developmental histories of beta-cells generate functional and proliferative heterogeneity
757 during islet growth. *Nat. Commun.* **8:** 664 Available at:
758 http://www.nature.com/articles/s41467-017-00461-3
759 Starlets D, Gore Y, Binsky I, Haran M, Harpaz N, Shvidel L, Becker-Herman S, Berrebi A &
760 Shachar I (2006) Cell-surface CD74 initiates a signaling cascade leading to cell
761 proliferation and survival. *Blood* **107:** 4807–4816
762 Szabat M, Page MM, Panzhinskiy E, Nislow C, Kieffer TJ, Johnson JD, Szabat M, Page MM,
763 Panzhinskiy E, Skovsø S, Mojibian M & Fernandez-tajes J (2016) Reduced Insulin
764 Production Relieves Endoplasmic Reticulum Stress and Induces b Cell Proliferation. *Cell*
765 *Metab.***:** 1–15 Available at: http://dx.doi.org/10.1016/j.cmet.2015.10.016
766 Tam AB, Mercado EL, Hoffmann A & Niwa M (2012) ER Stress Activates NF-??B by
767 Integrating Functions of Basal IKK Activity, IRE1 and PERK. *PLoS One* **7:**
768 Weir GC, Laybutt DR, Kaneto H, Bonner-weir S & Sharma A (2001) b-Cell Adaptation and
769 Decompensation During the Progression of Diabetes. *Diabetes* **50:** S154

770 Xiong Y, Yepuri G, Necetin S, Montani1 J-P, Ming X-F & Yang Z (2017) Arginase-II
771 promotes tumor necrosis factor-α release from pancreatic acinar cells causing β-cell
772 apoptosis in aging. *Diabetes* **66:** 1636–1649.
773 Yun M (2015) Changes in Regenerative Capacity through Lifespan. *Int. J. Mol. Sci.* **16:**
774 25392–25432 Available at: http://www.mdpi.com/1422-0067/16/10/25392/
775
776
777
778
779
780
781
782
783
784
785
786
787
788
789
790
791
792
793
794
795

796 **Figure legends:**

797 **Figure 1. Beta-cell proliferation declines with age**

798 (a) 3D-rendering of a primary islet from *Tg(ins:Fucci-G1);Tg(ins:Fucci-S/G2/M)* animals at 3
799 mpf showing nuclear *Tg(ins:Fucci-G1)* (red) and *Tg(ins:Fucci-S/G2/M)* (green) expression.
800 (b) Quantification of percentage of *Tg(ins:Fucci-S/G2/M)*-positive and *Tg(ins:Fucci-G1)*-
801 negative (green-only) beta-cells at 35 dpf (n=5), 3 mpf (n=9) and 1 ypf (n=10) animals. Each
802 dot represents one animal. Horizontal bars represent mean values (one-way ANOVA, *
803 $p<0.05$).
804 (c, d, e) Confocal projection of whole-mount islets from *Tg(ins:Fucci-G1);Tg(ins:Fucci-*
805 *S/G2/M)* animals at 35 dpf, 3 mpf and 1 ypf. Anterior to the top. Scale bar 50 µm.
806 (f) *Ex vivo* live-imaging of beta-cells from *Tg(ins:nlsRenilla-mKO2);Tg(ins:GCaMP6s)*
807 animals at 3 mpf. Beta-cells (red) were stimulated with 2.5 (basal) mM D-Glucose, (f') 11
808 mM D-glucose, (f'') 16.7 mM D-glucose and (f''') depolarized using 30 mM KCl while
809 monitoring GCAMP6s-fluorescence (green). Scale bar 10 µm.
810

811 **Figure 1-figure supplement 1.**
812 (a,b) Confocal projection of whole-mount secondary islets from *Tg(ins:Fucci-*
813 *G1);Tg(ins:Fucci-S/G2/M)* animals at 35 dpf, 3 mpf and 1 ypf. Scale bar 20 µm.
814 (c) Quantification of percentage of *Tg(ins:Fucci-S/G2/M)*-positive and *Tg(ins:Fucci-G1)*-
815 negative (green-only) beta-cells from 35 dpf (n=8, secondary islets=16), 3 mpf (n=8,
816 secondary islets=70) and 1 ypf (n=8, secondary islets=76) animals. Error bars show s.e.m.
817 (one-way ANOVA, * $p<0.05$).
818

819 **Figure 2. Transcriptome profiling of younger and older beta-cells**

820 (a) Schematic showing isolation and FAC-sorting of beta-cells from *Tg(ins:nlsRenilla-mKO2)*
821 animals at 3 mpf and 1 ypf followed by high-throughput mRNA-Sequencing.
822 (a') Heatmap depicting differentially regulated genes among the beta-cells at 1 ypf and 3 mpf
823 involved in beta-cell proliferation, function and inflammation (asterisk denotes genes
824 validated by single-cell RT-qPCR).
825 (b) Volcano plot representing the distribution of genes that were differentially regulated in
826 beta-cells from 1 ypf and 3 mpf (1.5-$\log_2$fold change, $p<0.05$).
827 (c) The biological categories of enriched genes in beta-cells at 1 ypf (1.5-$\log_2$fold change,
828 $p<0.05$) based on literature survey. (c') Unbiased gene-ontology analysis using DAVID of
829 genes enriched in beta-cells at 1 ypf ($p < 0.05$).
830 (d) Gene expression analysis was carried out using single-cell RT-qPCR. Violin plots denote
831 expression distribution of the candidate genes. The Y-axis shows
832 -$\log_{10}$(Ct) values of transcript levels in single beta-cells. The X-axis shows gene names and
833 the respective developmental stages. The percentage values under each violin plot denote the
834 proportion of beta-cells with detectable transcript levels. The cycle threshold for detectable
835 gene expression was set as Ct=40. The value -1.6 (-$\log_{10}$(40)) on the Y-axis represents
836 undetectable expression as measured by single-cell RT-qPCR (see Materials and Methods).
837 Each dot represents one beta-cell. Significance testing for differences in proportion of cells
838 with detectable gene expression at each stage was performed using Pearson's Chi-Square test
839 (**$p<0.01$, ***$p<0.001$).
840
841 **Figure 2-figure supplement 1.**
842 (a) Fluorescent activated cell sorting (FACS) of RFP-positive and calcein-positive beta-cells
843 from *Tg(ins:nlsRenilla-mKO2)* animals.
844

845 **Figure 3. An inflammation reporter reveals heterogeneous activation of NF-kB**
846 **signaling in beta-cells with age**
847 (a) The images show single confocal planes from islets of 5 dpf larvae. The *tnfrsf1b* coding
848 sequence was expressed under the control of the insulin promoter. The plasmid was injected
849 in *Tg(NF-kB:GFP)* embryos at the one-cell-stage, leading to mosaic and stochastic expression
850 of the construct in beta-cells. The *Tg(NF-kB:GFP)* reporter expresses GFP (green) under the
851 control of six tandem repeats of NF-kB DNA-binding sites. Beta-cells were labelled using an
852 insulin antibody (red). Arrows indicate GFP-positive beta-cells. Scale bar 5 µm.
853 (b) The graph shows the percentage of GFP-positive and insulin-positive cells in uninjected
854 controls (n=5) and *tnfrsf1b* injected animals (n=6) at 5 dpf. Horizontal bars represent mean
855 values.
856 (c-e) Confocal stack of islets from *Tg(NF-kB:GFP)* animals at 1 mpf, 3 mpf and 1ypf. Beta-
857 cells were labelled using an insulin antibody (red). *NF-kB*:GFP reporter expression is shown
858 in green. Scale bars 20 µm.
859 (c'-e') Insets show high magnification single planes of the confocal stacks (corresponding to
860 the regions shown using white dotted-lines in the top panels). Scale bar 10 µm.
861 (f-g) Beta-cells from 3 mpf *Tg(NF-kB:GFP)* animals were labelled with TSQ (Zn2+ labelling
862 dye) and analyzed using FACS. The graph shows GFP intensity (along the X-axis) and the
863 distribution of beta-cells at 3 mpf and 1 ypf. Horizontal lines indicate the division point
864 between GFP^{low} and GFP^{high} levels. Percentage values represent proportion of cells with
865 GFP^{low} or GFP^{high} expression.
866
867 **Figure 3-figure supplement 1.**
868 (a,b,c) Confocal stack of secondary islets from *Tg(NF-kB:GFP)* animals at 1 mpf, 3 mpf and
869 1 ypf. Beta-cells were labelled using an insulin antibody (red). *NF-kB*:GFP reporter
870 expression is shown in green. Scale bars 20 µm.

871 (a',b',c') Insets show high magnification single planes of the confocal stacks corresponding
872 to the regions outlined using white dotted-lines in the top panels. Scale bar 10 µm.
873 (d) Graph showing the total normalized GFP fluorescence intensity of the secondary islets
874 from 3 mpf (n=9, secondary islets=32) and 1 ypf (n=8, secondary islets=30) animals. Each
875 dot represents one islet (two-tailed t-test, * $p<0.05$).
876
877 **Figure 3-figure supplement 2.**
878 (a) Confocal image of dissociated cells from 3 mpf *Tg(ins:nlsRenilla-mKO2)* animals that
879 were labelled with TSQ (Zn^{2+} labelling dye). Islets were incubated with TSQ after
880 dissociation and imaged using a confocal microscope. Beta-cells show RFP expression (red)
881 while cells rich in Zn^{2+} are labelled with TSQ (cyan). TSQ strongly labels all beta-cells and
882 weakly labels some unknown endocrine cells.
883 (b) Fluorescent activated cell sorting (FACS) of live TSQ-positive GFP^{high} and GFP^{low} cells
884 from *Tg(NF-kB:GFP)* animals at 3 mpf and 1 ypf. Dead cells were labelled using far-red
885 stain DRAQ7.
886
887 **Figure 3-figure supplement 3.**
888 (a) Graph showing the relative fold change increase in EGFP mRNA levels in beta-cells from
889 1 ypf compared to 3 mpf animals, as measured using RT-qPCR (n=5 biological replicates
890 from three fish each, 1000 cells for each condition). Error bars show SD (two-tailed paired t-
891 test, * $p<0.05$).
892 (b) The graph shows the fluorescence levels of individual FAC-sorted beta-cells from *Tg(nF-*
893 *kB:GFP);Tg(ins:mCherry)* animals as $\log_{10}$(GFP intensity) (along the Y-axis) and Expression
894 threshold (Et) values of GFP mRNA (along X-axis) measured using single-cell RT-qPCR.
895 Line indicates the correlation between GFP fluorescence intensity and GFP-mRNA
896 expression levels in single cells. Each dot represents one beta-cell. $R^2=0.28$.

897

898 **Figure 4. Immune cells infiltrate the islet during early stages of development and persist**

899 **throughout adult life**

900 (a) Confocal images of pancreata from 15, 21 and 45 dpf animals. Beta-cells were labelled

901 using an insulin antibody (grey), leukocytes were labelled using an L-plastin antibody

902 (magenta) and *Tg*(*ptf1a:*GFP) marks the acinar cells (green). Immune cells are present within

903 the islet at 45 dpf (arrows).

904 (b) Confocal images of whole islets from *Tg(tnfα:GFP)* animals at 1 ypf. Islets were labelled

905 using TSQ (Zn^{2+} labelling dye) (blue), leukocytes were labelled with an L-plastin antibody

906 (magenta) and *Tg*(*tnfα:*GFP*)* marks cells expressing *tnfα* (green). Scale bars 20 µm.

907 (b') Insets show high magnification single planes from the confocal stacks (corresponding to

908 the area marked using a white dotted-line in b). Scale bar 10 µm.

909 (c-c') Confocal image of a 1 ypf islet showing a single plane. The *TgBAC(tnfα:GFP)* line

910 marks the *tnfα*-positive cells (green), whereas *Tg(mpeg1:mCherry)* marks the macrophages

911 (red). The L-plastin antibody marks all leukocytes (grey) and TSQ (Zn2+ labelling dye) was

912 used to mark the islet (n=5). Scale bar, 10 µm.

913 (d) Confocal images showing islets at 5 dpf. The *tnfα* cDNA was expressed under the insulin

914 promoter. The plasmid was injected in *Tg(NF-kB:GFP)* embryos at the one-cell-stage and the

915 islets were analyzed at 5 dpf. Beta-cells were labelled with an insulin antibody (red). *Tg(NF-*

916 *kB*:GFP) reporter expression is shown in green.

917 (e) The graph shows the percentage of GFP and insulin double-positive cells in un-injected

918 controls (n=7) and *ins:tnfα* injected animals (n=8) at 5 dpf. Horizontal bars represent mean

919 values (two-tailed t-test, * $p<0.05$).

920

921 **Figure 4-figure supplement 1.**

922 (a,a') Confocal image of a juvenile islet. *Tg(ins:CFP-NTR)* line marks the beta-cells with
923 CFP (green), leukocytes were labelled with the L-plastin antibody (blue) and
924 *Tg(mpeg1:mCherry)* marks the macrophages (red).
925 (b) Quantification of the percentage of *TgBAC(tnfa:*GFP*)* and L-plastin double-positive cells
926 over the total number of L-plastin-positive cells in the islets of *TgBAC(tnfa:GFP)* animals at 3
927 mpf (n=5) and 1 ypf (n=5). Horizontal bars represent mean values (two-tailed t-test, p>0.05).
928 (c) Quantification of the total number of *TgBAC(tnfa:*GFP*)*-positive and L-plastin double-
929 positive cells at 3 mpf (n=5) and 1 ypf (n=5). Horizontal bars represent mean values (two-
930 tailed t-test, p>0.05).
931 (d) Quantification of the total number of L-plastin positive and positive cells at 3 mpf (n=5)
932 and 1 ypf (n=5). Horizontal bars represent mean values (two-tailed t-test, p>0.05).
933
934 **Figure 5. *NF-kB*:GFP^{high} beta-cells proliferate less than their neighbors**
935 (a) Schematic showing the EdU (5-ethynyl-2′-deoxyuridine) incorporation assay. *Tg(NF-*
936 *kB:GFP)* animals were incubated in EdU at 3 mpf for two consecutive nights and fed during
937 each day.
938 (b) EdU incorporation assay was performed to mark the proliferating beta-cells in *Tg(NF-*
939 *kB:GFP)* animals at 3 mpf. The confocal image (single plane) shows an overview of a section
940 through the islet. Beta-cells were labelled with an insulin antibody (red), a GFP antibody
941 (green) and EdU (blue). Arrowheads point to EdU-positive beta-cells.
942 (b'-b'') The insets show higher magnification images with and without the EdU channel.
943 EdU incorporation can be observed in some of the GFP^{low} cells (white arrow-heads).
944 (c) An insulin-positive cell was first located by going through individual sections in the
945 confocal z-stack. The optical section containing the largest area of the nucleus was chosen as
946 the center of the cell. A region-of-interest (ROI) was drawn around the nucleus and the
947 fluorescence intensities of the GFP and DAPI channels were recorded. The normalized GFP

948 intensity was calculated as a ratio of mean GFP intensity and mean DAPI intensity for each
949 ROI. The average total normalized GFP-intensity of each islet was set as a threshold for
950 dividing the cells into GFP^{high} and GFP^{low} populations. The graph shows the percentage of
951 EdU and insulin double-positive cells among the GFP^{high} and GFP^{low} populations. Each dot
952 represents one islet (n=9). Horizontal bars represent mean values (two-tailed t-test, * $p<0.05$).
953 (d) The graph shows the percentage of PCNA and insulin double-positive cells among the
954 GFP^{high} and GFP^{low} populations. Each dot represents one islet (n=13). Horizontal bars
955 represent mean values (two-tailed t-test, * $p<0.05$). See also Figure 5-figure supplement 2 for
956 representative PCNA antibody staining.
957
958 **Figure 5-figure supplement 1.**
959 (a,b,c) Beta-cells from *Tg(NF-kB:GFP);Tg(ins:mCherry)* animals at 3 mpf were FAC-sorted
960 as single cells in 384-well plates and followed over 72 hours. *NF-kB*:GFP^{high} cells at 24, 48
961 and 72 hours post FAC-sorting. Scale bar 5 µm.
962 (a',b',c') *NF-kB*:GFP^{low} cells at 24, 48 and 72 hours post FAC-sorting. The GFP intensity
963 remains stable over at least 72 hours. Scale bar 5 µm.
964 (d) Quantification showing the mean GFP fluorescence intensity of GFP^{high} and GFP^{low} cells
965 (n=7 GFP^{high} cells and n=5 GFP^{low} cells).
966
967 **Figure 5-figure supplement 2.**
968 (a) Islets were stained for PCNA to mark the proliferating beta-cells in *Tg(NF-kB:GFP)*
969 animals at 3 mpf. The confocal image (single plane) shows an overview of a section through
970 the islet. The sections were stained with an insulin antibody (red), a GFP antibody (green)
971 and PCNA (blue).
972 (a'-a'') The insets show higher magnification images. PCNA incorporation can be observed
973 in some of the GFP^{low} cells (white arrow-heads).

974 **Figure 6. *Socs2* is enriched in *NF-kB*:GFP^{high} cells and inhibits beta-cell proliferation in**
975 **a cell-autonomous manner**
976 (a) Schematic showing the sorting of beta-cells from the double transgenic line
977 *Tg(ins:mCherry);Tg(NF-kB:GFP)* at 3 mpf into GFP^{high} and GFP^{low} cells using FACS.
978 (b) Bulk RT-qPCR was performed on the GFP^{high} and GFP^{low} beta-cells (n=3 to 4 biological
979 replicates, n=3 animals per replicate, 1000 cells per condition). Candidate genes significantly
980 enriched in beta-cells at 1 ypf were chosen to be compared between the GFP^{high} and GFP^{low}
981 populations at 3 mpf. The graph shows relative fold-change between GFP^{high} and GFP^{low}
982 cells. The expression of all genes was normalized to β-actin expression before calculating
983 fold-change. *socs2* shows higher expression in the GFP^{high} cells. Error bars, SD (two-tailed
984 paired t-test, * $p<0.05$).
985 (c) Schematic showing the method for mosaic overexpression of candidate genes in beta-
986 cells. The *socs2* coding sequence is linked to nuclear-CFP using a T2A sequence. The entire
987 construct was expressed under the insulin promoter. This construct was injected in one-cell-
988 stage-embryos from *Tg(ins:Fucci-G1);Tg(ins:Fucci-S/G2/M)* animals leading to mosaic and
989 stochastic expression of *socs2* in beta-cells during islet development. Control animals were
990 injected with plasmid containing only nuclear-CFP sequence (See Figure 6-figure supplement
991 2).
992 (d) Confocal projections showing mosaic expression of *socs2-T2A-CFP (blue)* at 23 dpf
993 (blue). Proliferating beta-cells are marked by *Tg(ins:Fucci-S/G2/M)* expression (green) and
994 absence of *Tg(ins:Fucci-G1)* expression (red). Anterior to the left. Scale bar 10 µm.
995 (d') Insets show higher magnification single planes from the confocal stacks (white dotted-
996 line in d) with separate channels. The proliferating beta-cells are CFP-negative (yellow
997 arrowheads) whereas some of the non-proliferating cells are CFP-positive (white arrowheads)
998 (e) Quantification of the percentage of *Tg(ins:FUCCI-S/G2/M)*-positive and *Tg(ins:FUCCI-*
999 *G1)*-negative (green only) beta-cells. The *socs2* expressing β-cells exhibit reduced cell-cycle

1000 progression compared to wild-type neighbors (n=9). Horizontal bars represent mean values

1001 (two-tailed t-test, * $p<0.05$).

1002

1003 **Figure 6-source data 1.** This spreadsheet contains the Relative Fold Change between NF-

1004 kB:GFP^{high} and NF-kB:GFP^{low} beta-cells used to generate the bar plots and average data

1005 shown in Figure 6b.

1006

1007 **Figure 6-figure supplement 1.**

1008 (a) Contour plot showing FACS of live RFP-positive GFP^{high} and GFP^{low} cells from *Tg(NF-*

1009 *kB:GFP);Tg(ins:mCherry)* animals at 3 mpf. Live cells were labelled with calcein.

1010 (b) Dot plot shows FACS of live RFP-positive GFP^{high} and GFP^{low} cells from *Tg(NF-*

1011 *kB:GFP);Tg(ins:mCherry)* animals at 3 mpf.

1012

1013 **Figure 6-figure supplement 2.**

1014 (a,b,c) Confocal images showing mosaic expression of nuclear-CFP (a), CFP-T2A-*spry4* (b)

1015 and CFP-T2A-*rapgef4* (c) at 23 dpf. *Tg(ins:Fucci-G1)* expression is shown in red,

1016 *Tg(ins:Fucci-S/G2/M)* expression in green and CFP expression in blue. Anterior to the top.

1017 Scale bar 20 µm.

1018 (a',b',c') Quantification of the percentage of *Tg(ins:FUCCI-S/G2/M)*-positive and

1019 *Tg(ins:FUCCI-G1)*-negative (green only) beta-cells among the CFP-positive and CFP-

1020 negative sub-populations for each experiment shown in the left-hand panels. Horizontal bars

1021 represent mean values (two-tailed t-test, $p > 0.05$).

1022

1023 **Figure 7. A schematic summarizing our model.**

1024 Beta-cell proliferation declines with age together with a concurrent increase in NF-kB

1025 signaling. The activation of NF-kB signaling is heterogeneous among beta-cells and

1026 correlates with their proliferative heterogeneity. In particular, beta-cells with higher NF-kB
1027 activity proliferate less compared to neighbors with lower activity, and express higher levels
1028 of *socs2*, which can inhibit beta-cell proliferation. Furthermore, the crosstalk with *tnfα*-
1029 positive immune cells in the islet provides a potential source of inflammation and NF-kB
1030 activation in beta-cells.

1031
1032 **Supplementary File 1.** List of genes differentially expressed from RNA-Seq of beta-cells at 3
1033 mpf and 1 ypf ($\log_2$FC ±1.5).

1034

1035 **Supplementary File 2.** List of primer sequences of genes validated using single-cell RT-
1036 qPCR and bulk RT-qPCR.

1037

Figure 1

Tg (ins:FUCCI-G1); *Tg (ins:FUCCI-S/G2/M)*

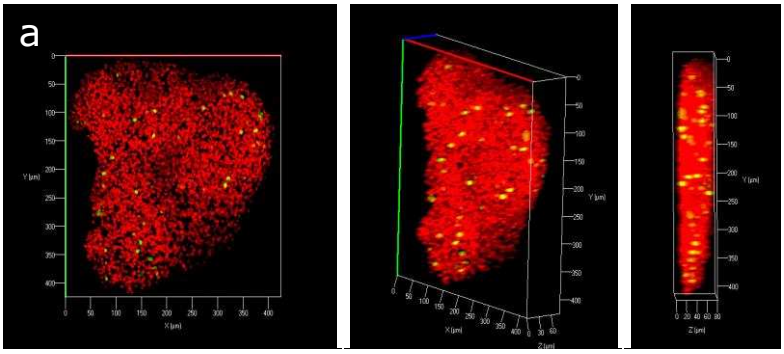

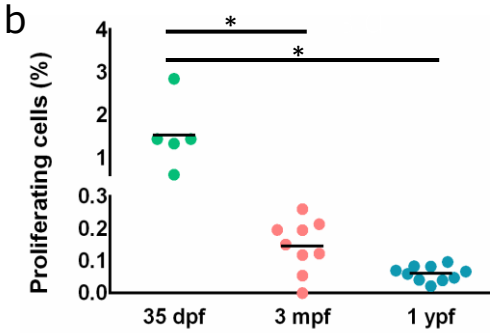

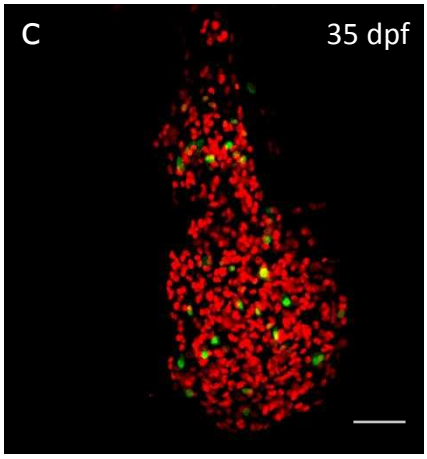

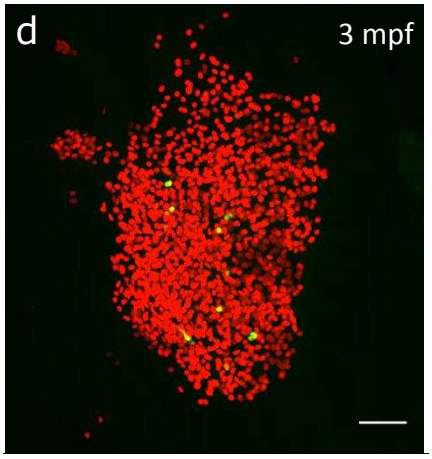

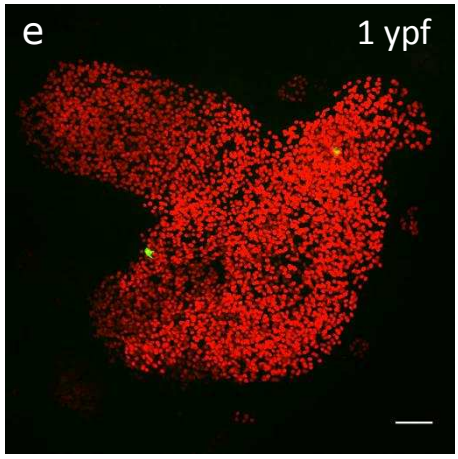

Tg(ins:mKO2); *Tg(ins:GCAMP6s)*

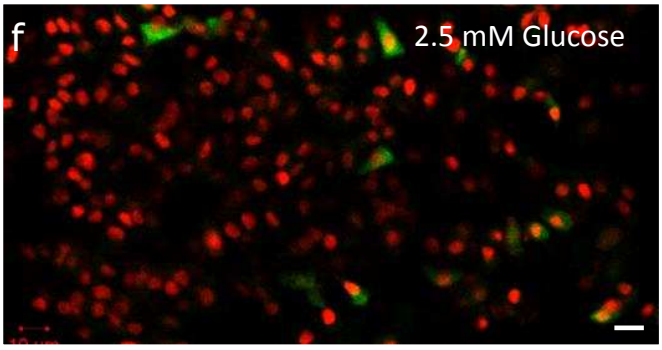

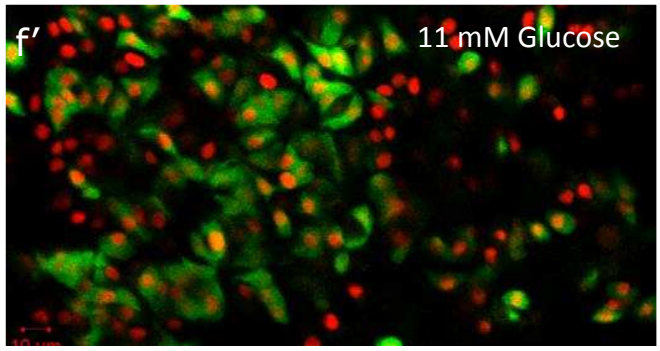

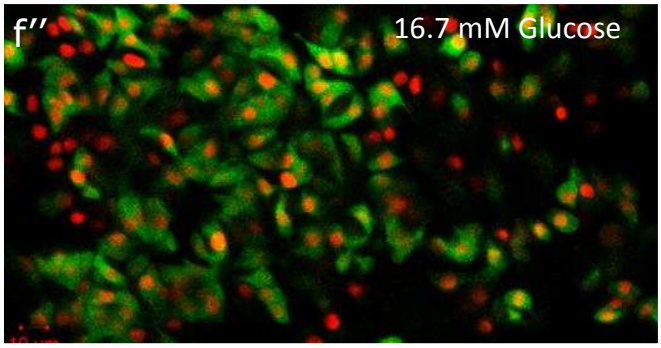

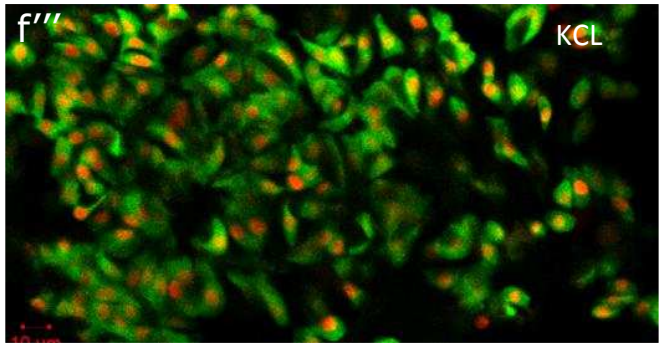

Figure 1 – figure supplement 1

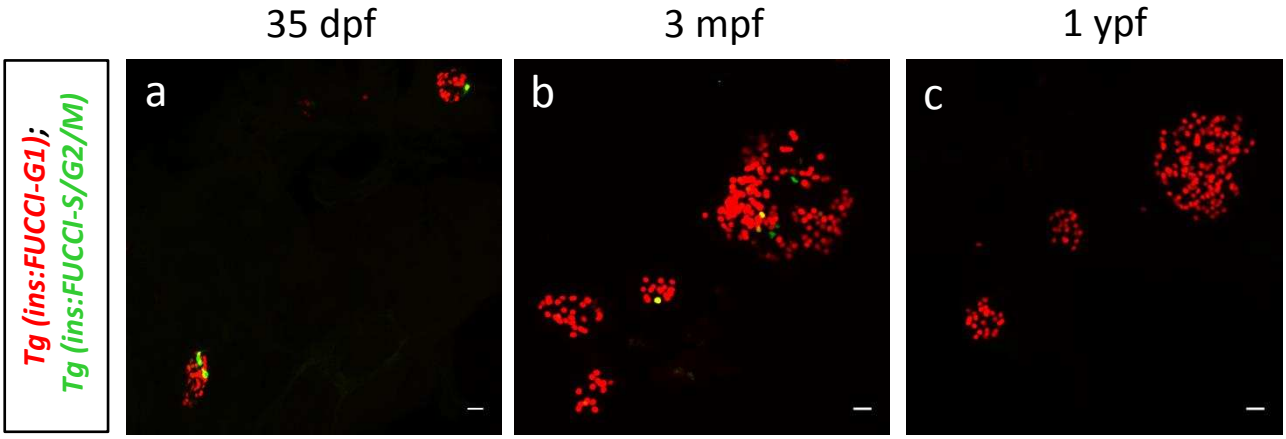

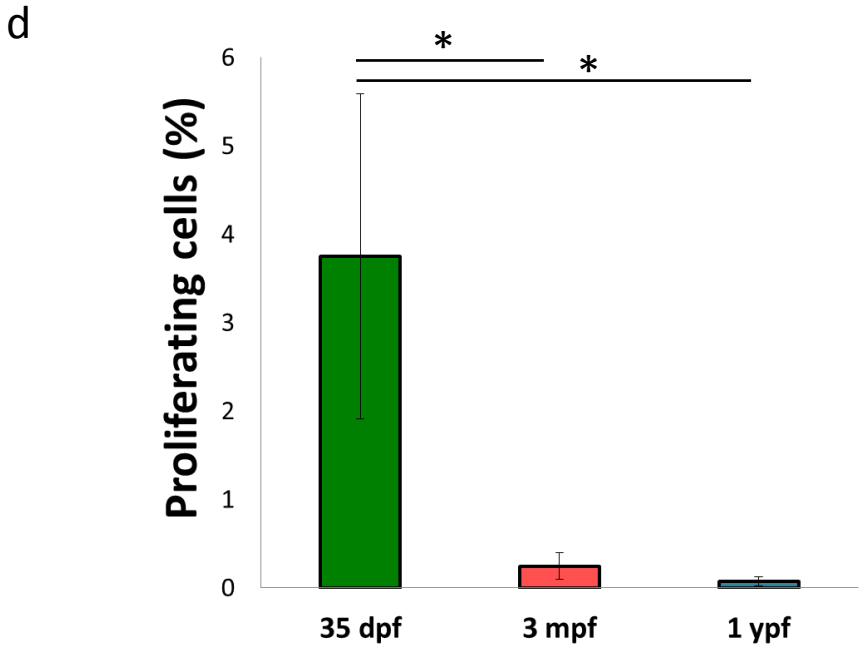

Figure 2

a

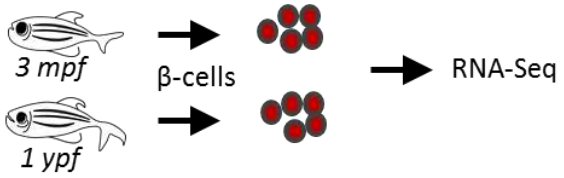

a'

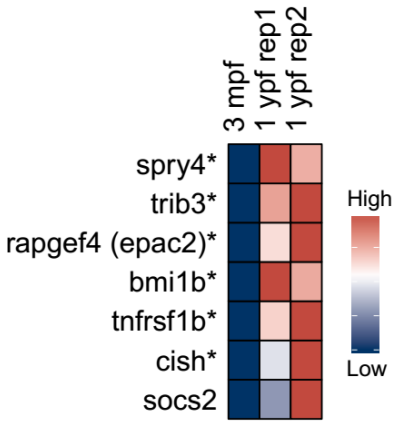

b

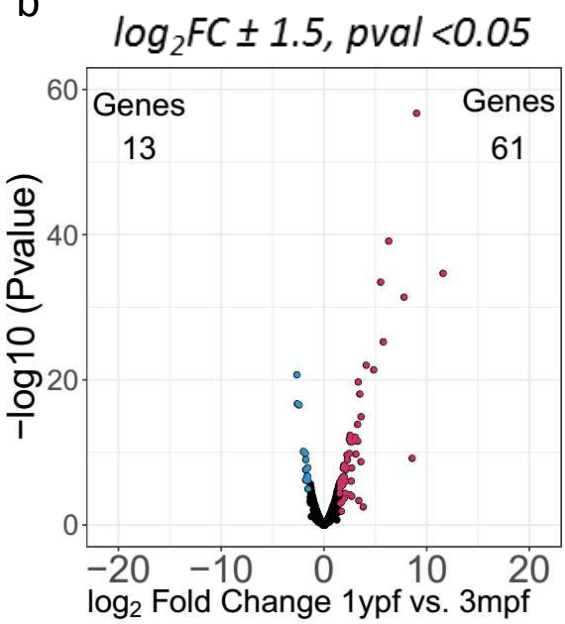

c

Category	Genes
Negative regulation of growth factor signaling	socs2, cish, spry4, fstl1
Glucose intolerance/variants linked to T2D	prtfa, lpp, socs2
ER stress	trib3, cebpd
Beta-cell function and proliferation	epac4, dio3, irs2, bmi1b
Inflammation and response to immune system	il15, tnfrsf1b, c9, cd74a, cd74b

c'

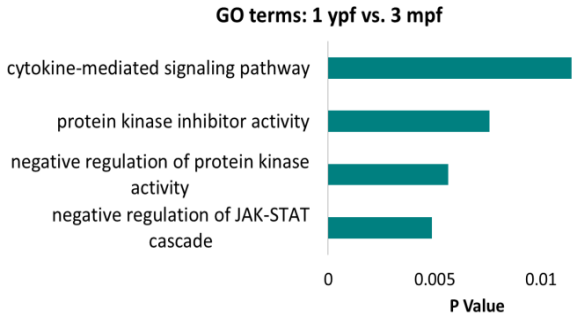

d

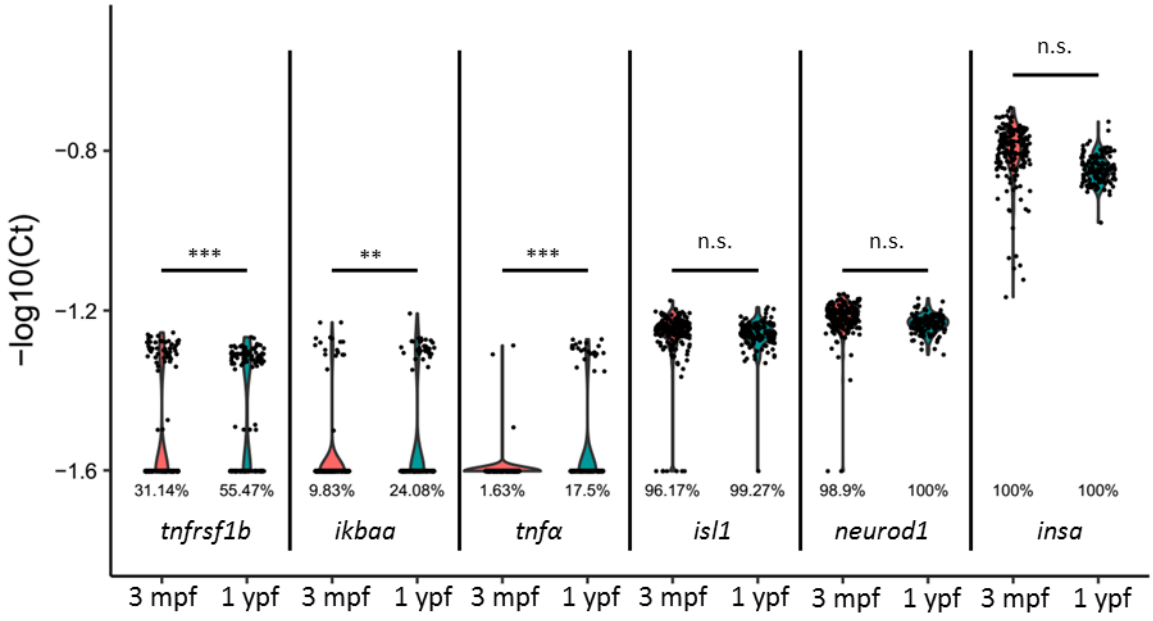

Figure 2 – figure supplement 1

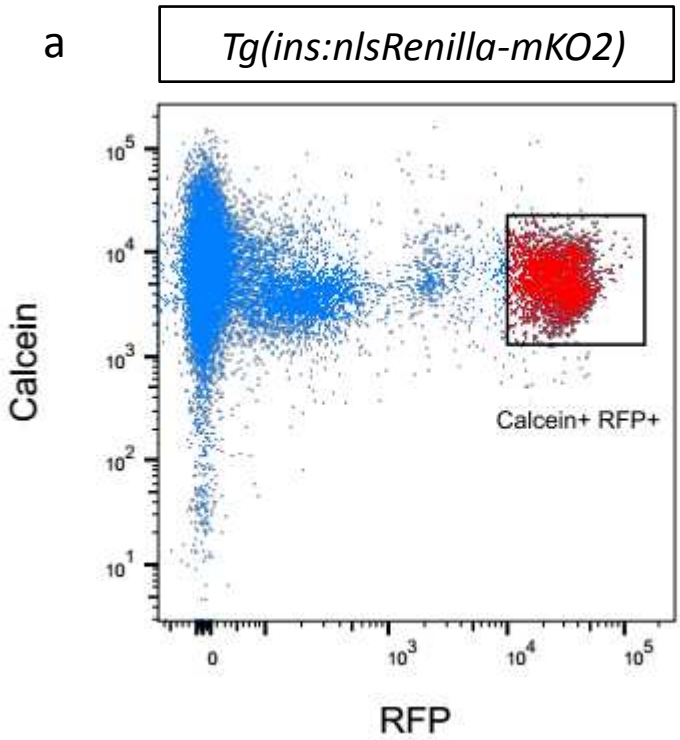

Figure 3

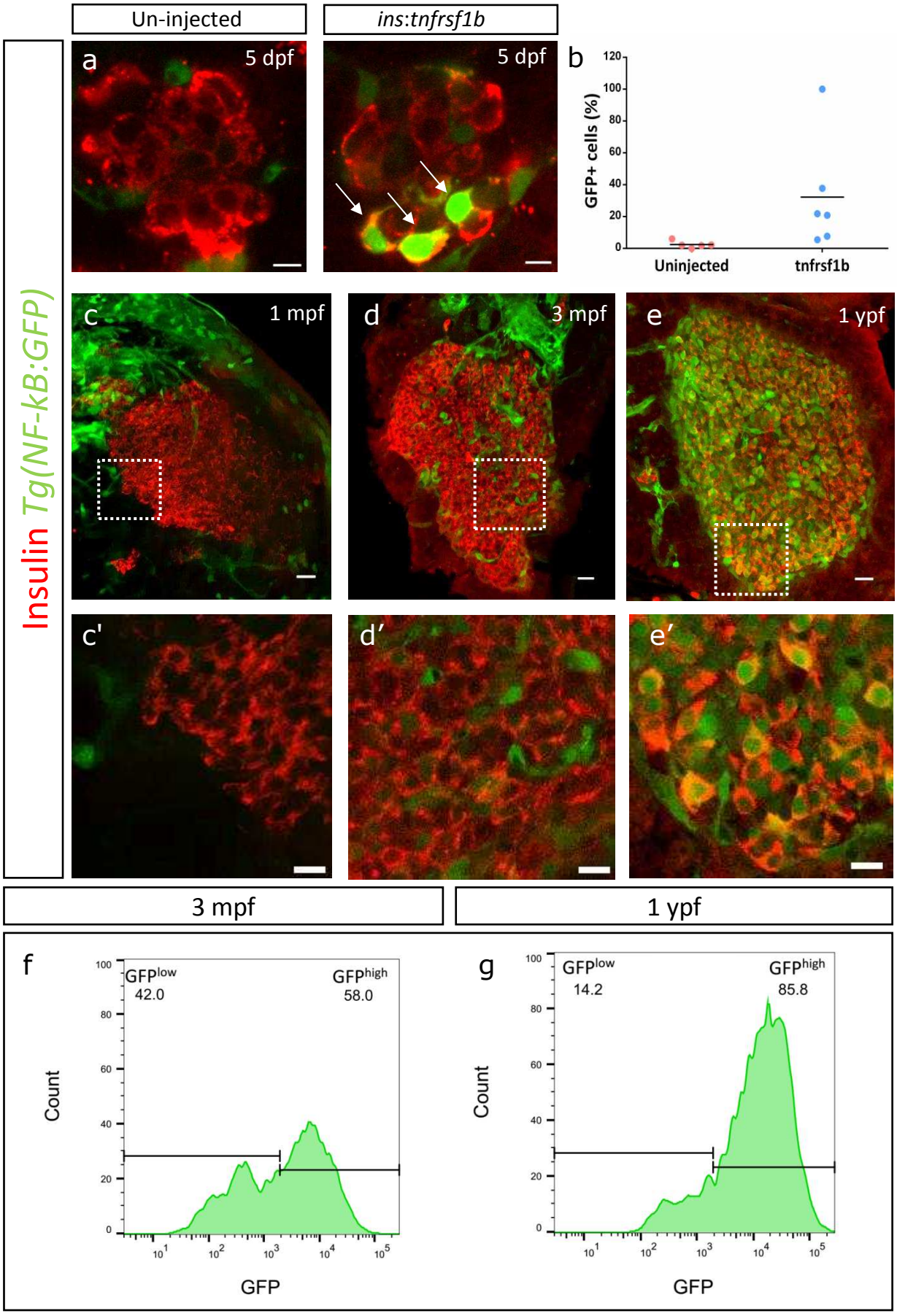
Un-injected
ins:tnfrsf1b
Insulin Tg(NF-kB:GFP)
a
5 dpf
5 dpf
b
GFP+ cells (%)
Uninjected
tnfrsf1b
c
1 mpf
d
3 mpf
e
1 ypf
c'
d'
e'
3 mpf
1 ypf
f
GFPlow
42.0
GFPhigh
58.0
Count
GFP
g
GFPlow
14.2
GFPhigh
85.8
Count
GFP

Figure 3 – figure supplement 1

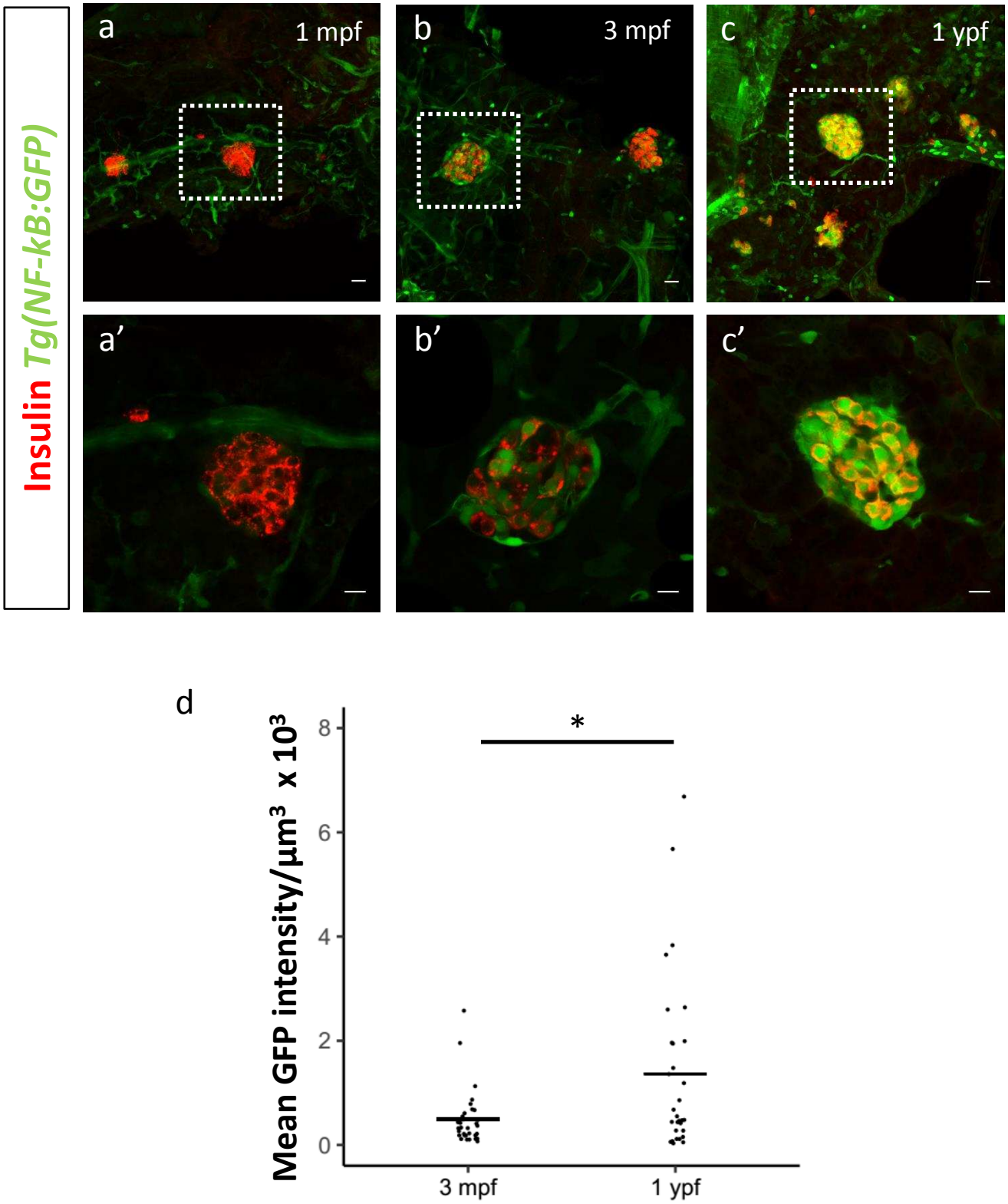

Figure 3 – figure supplement 2

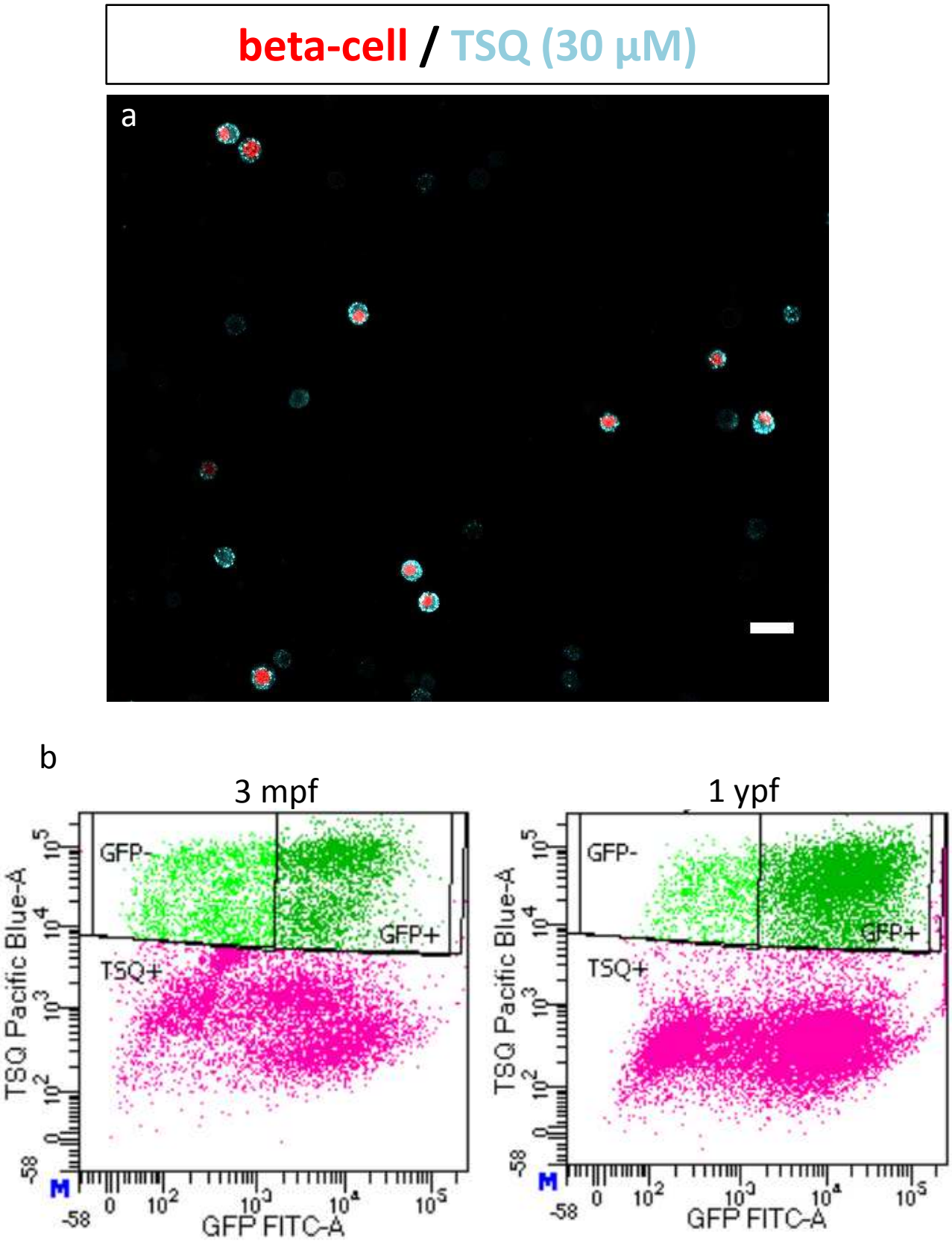

Figure 3 – figure supplement 3

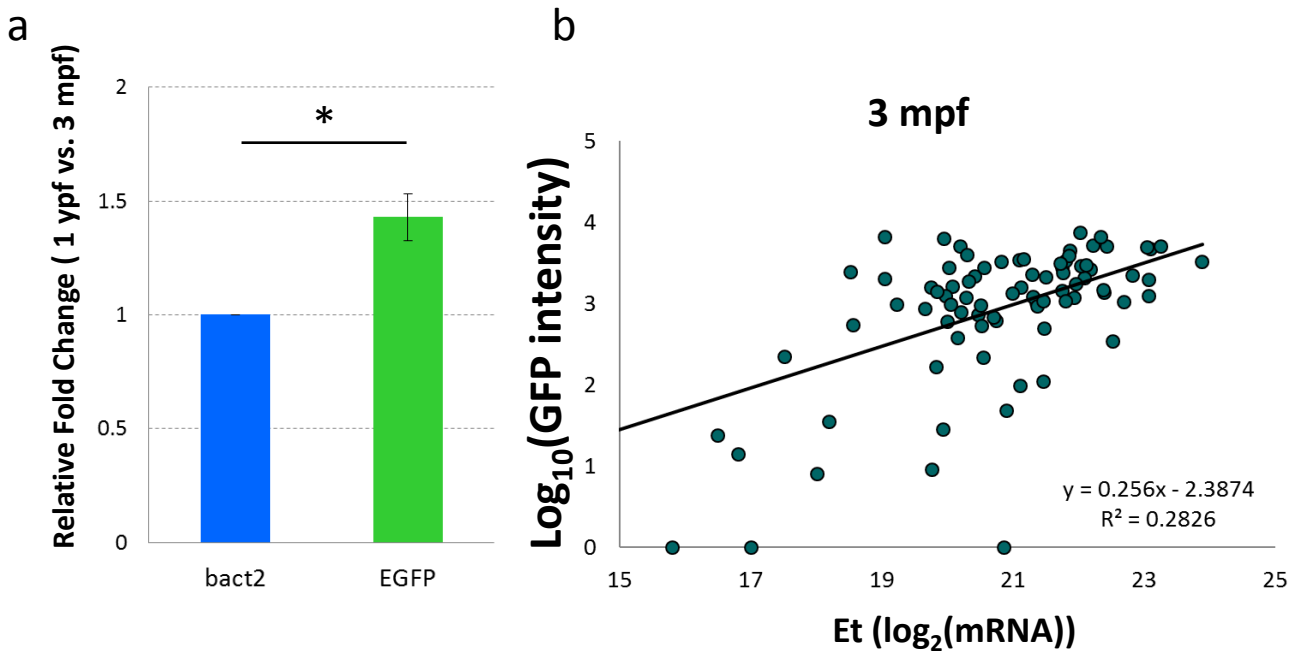

Figure 4

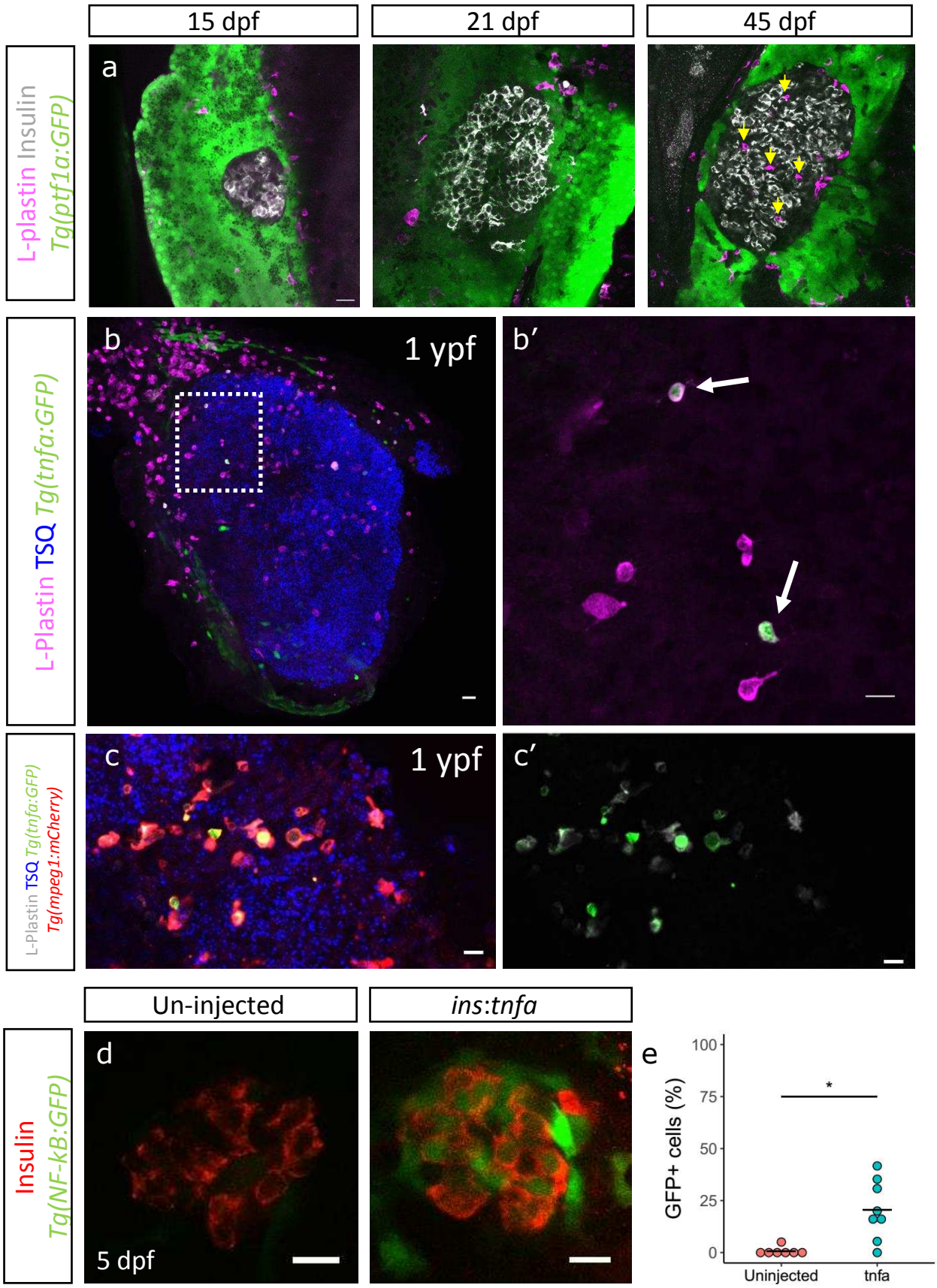
15 dpf
21 dpf
45 dpf
L-plastin Insulin
Tg(ptf1a:GFP)
a
b
1 ypf
b′
L-Plastin TSQ Tg(tnfa:GFP)
c
1 ypf
c′
L-Plastin TSQ Tg(tnfa:GFP)
Tg(mpeg1:mCherry)
Un-injected
ins:tnfa
Insulin
Tg(NF-kB:GFP)
d
5 dpf
e
GFP+ cells (%)
100
75
50
25
0
*
Uninjected
tnfa

Figure 4 – figure supplement 1

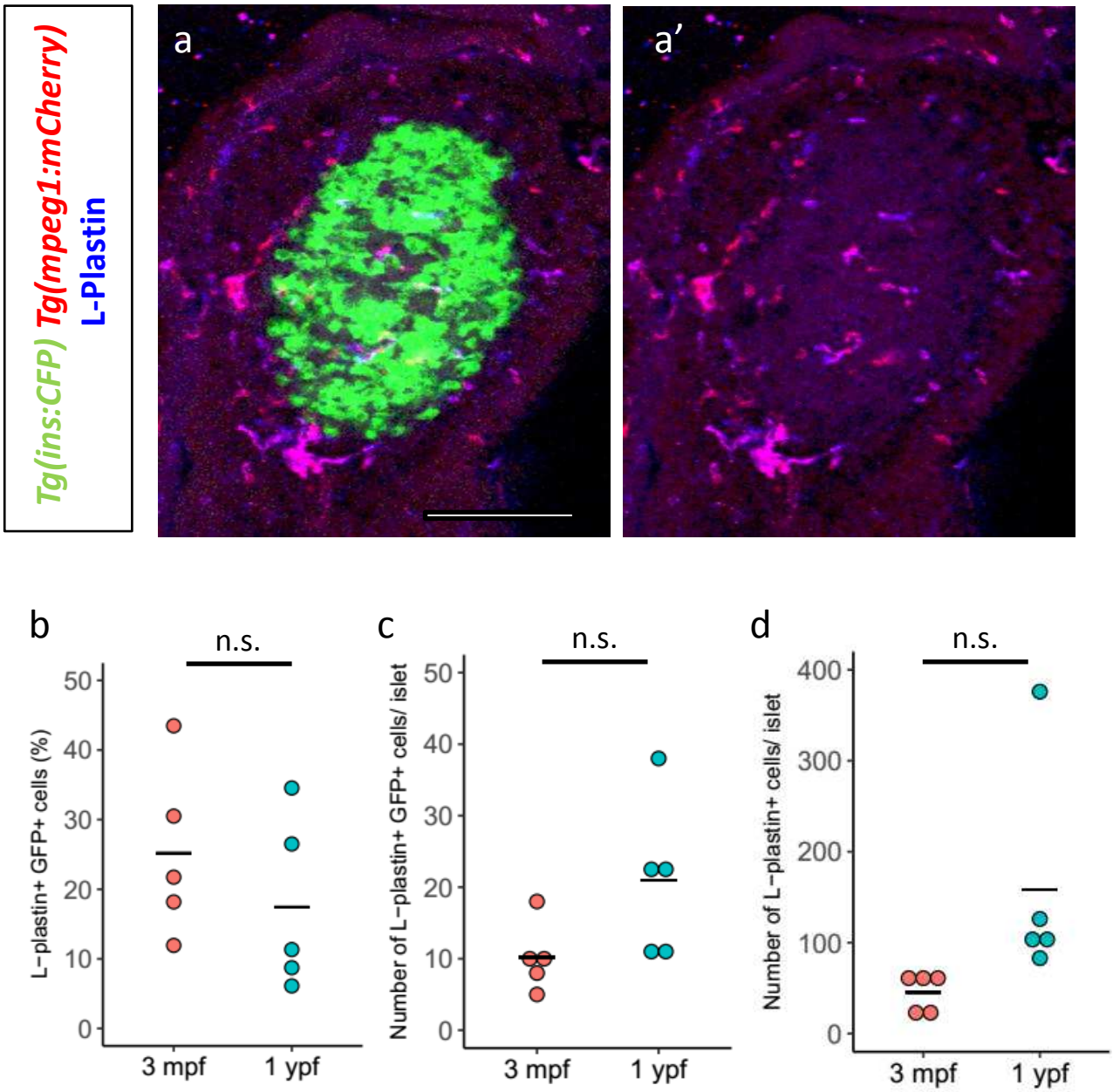

Figure 5

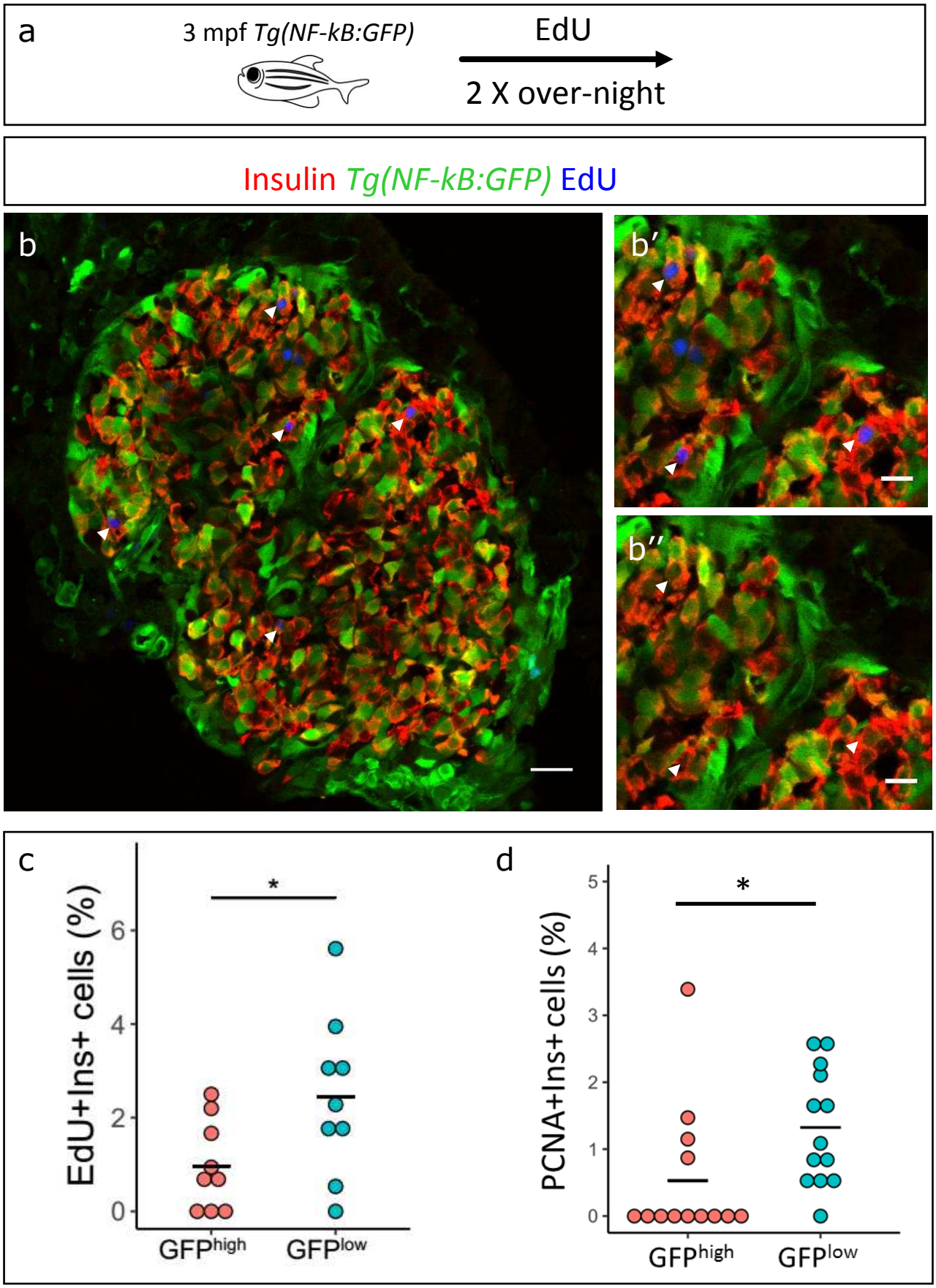
a
3 mpf Tg(NF-kB:GFP)
EdU
2 X over-night
Insulin Tg(NF-kB:GFP) EdU
b
b′
b″
c
EdU+Ins+ cells (%)
0
2
4
6
*
GFPhigh
GFPlow
d
PCNA+Ins+ cells (%)
0
1
2
3
4
5
*
GFPhigh
GFPlow

Figure 5 – figure supplement 1

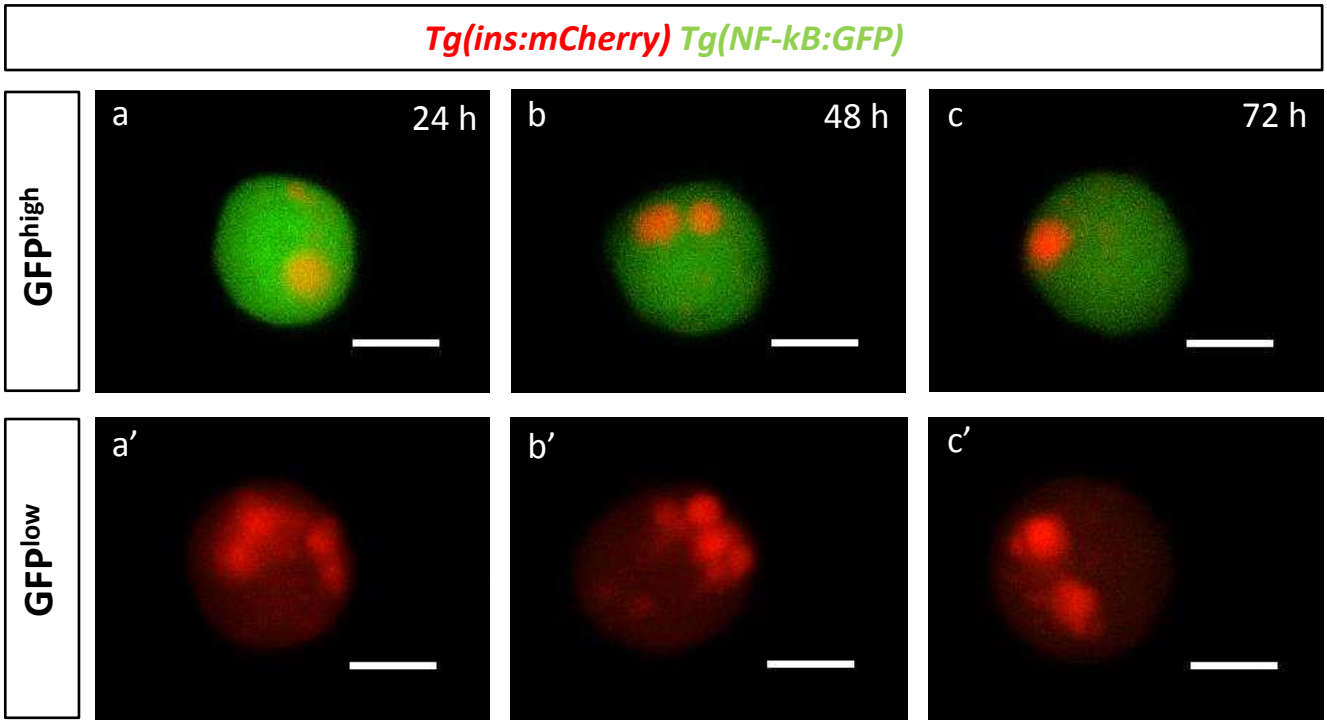

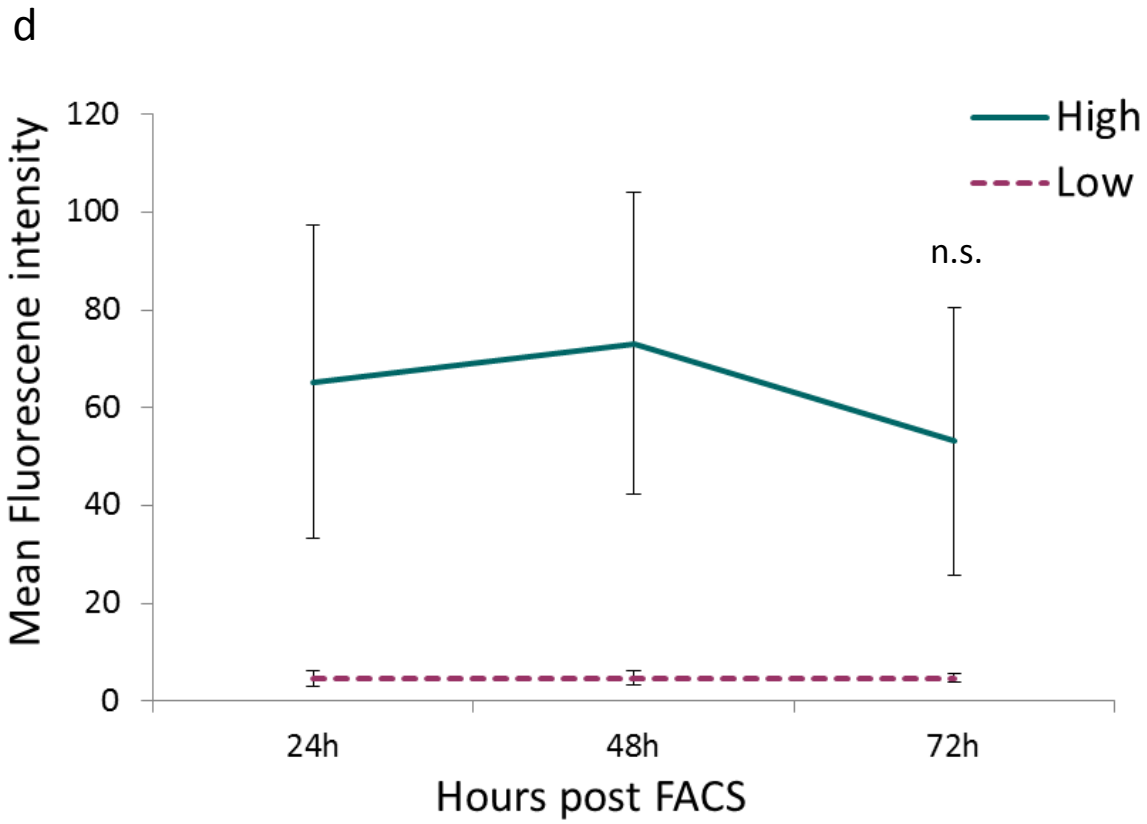

Figure 5 – figure supplement 2

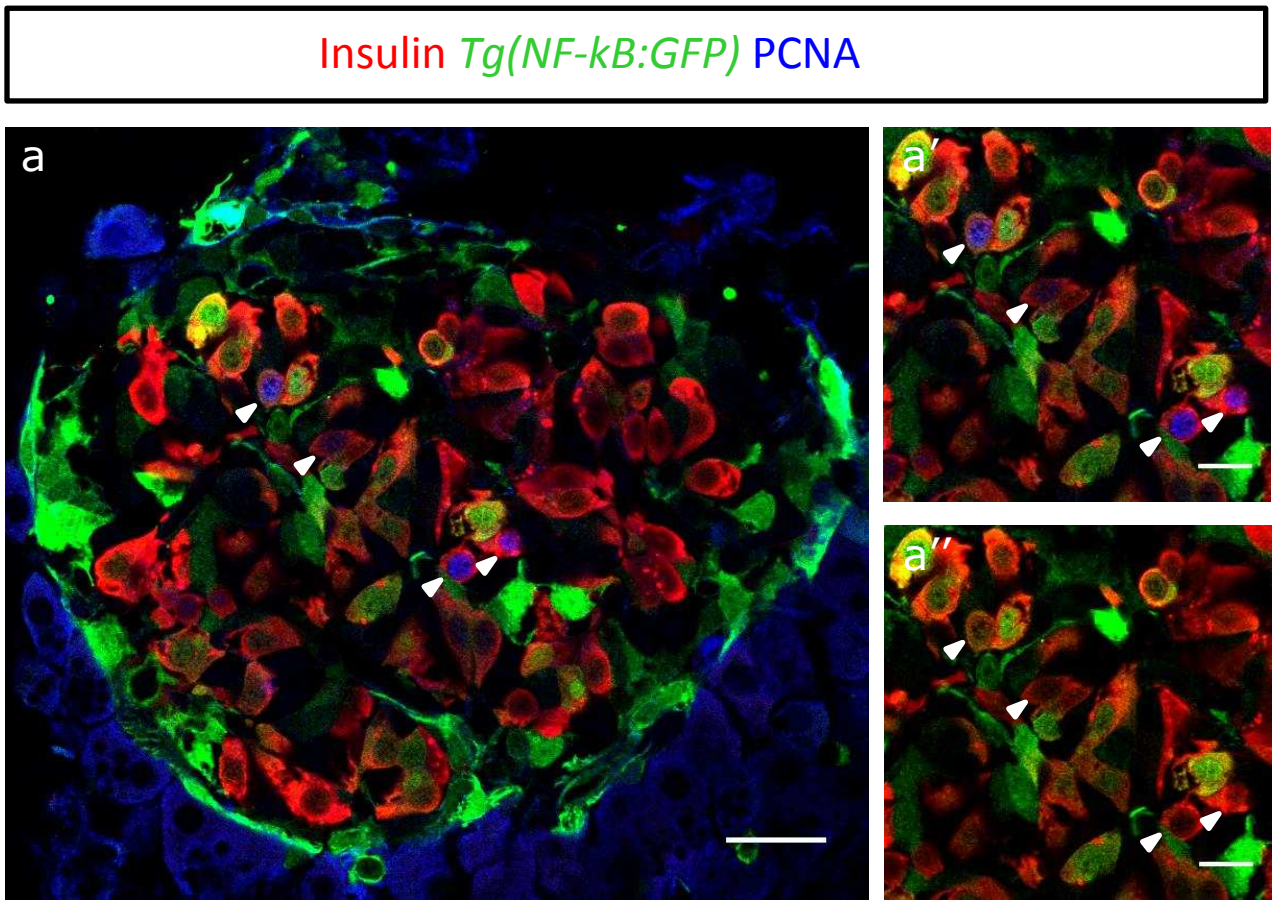

Figure 6

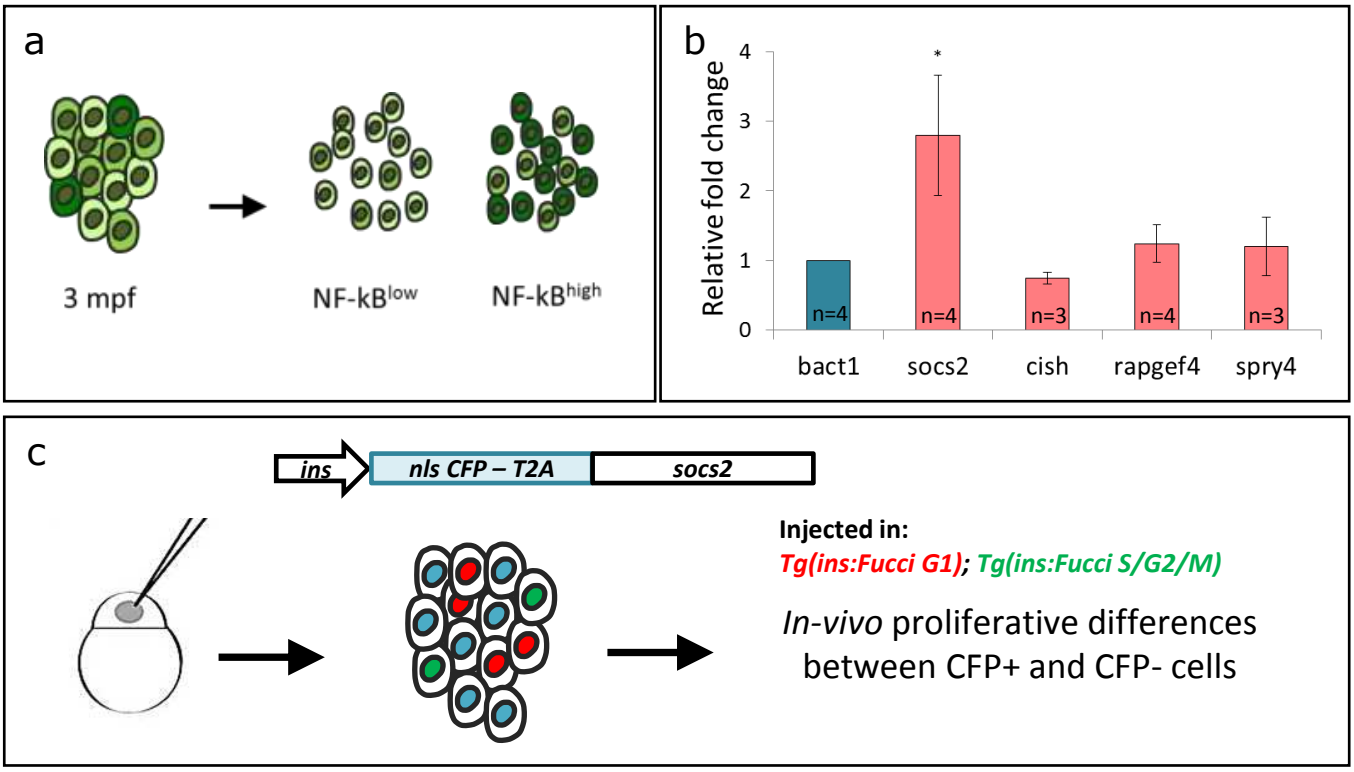
a
3 mpf
NF-kB^{low}
NF-kB^{high}
b
Relative fold change
0
1
2
3
4
*
n=4
n=4
n=3
n=4
n=3
bact1
socs2
cish
rapgef4
spry4
c
ins
nls CFP – T2A
socs2
Injected in:
Tg(ins:Fucci G1); Tg(ins:Fucci S/G2/M)
In-vivo proliferative differences between CFP+ and CFP- cells

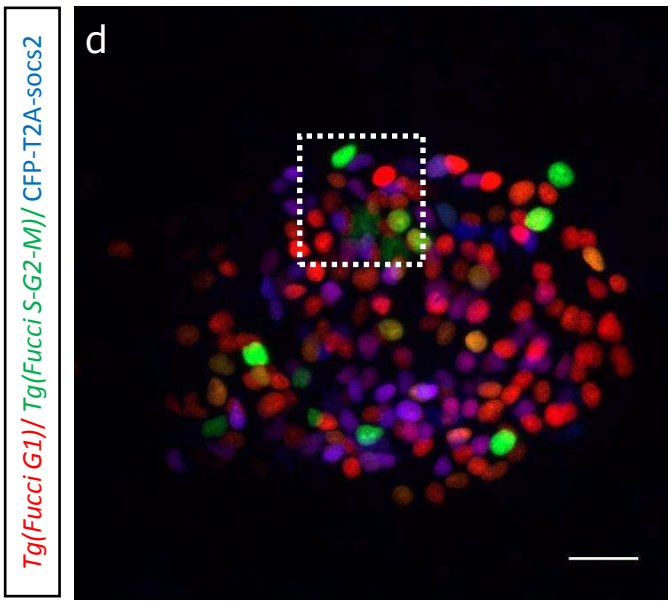
Tg(Fucci G1)/ Tg(Fucci S-G2-M)/ CFP-T2A-socs2
d

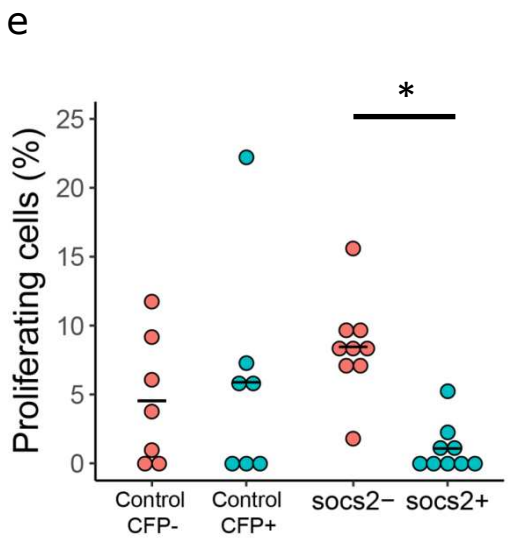
e
Proliferating cells (%)
0
5
10
15
20
25
*
Control CFP-
Control CFP+
socs2−
socs2+

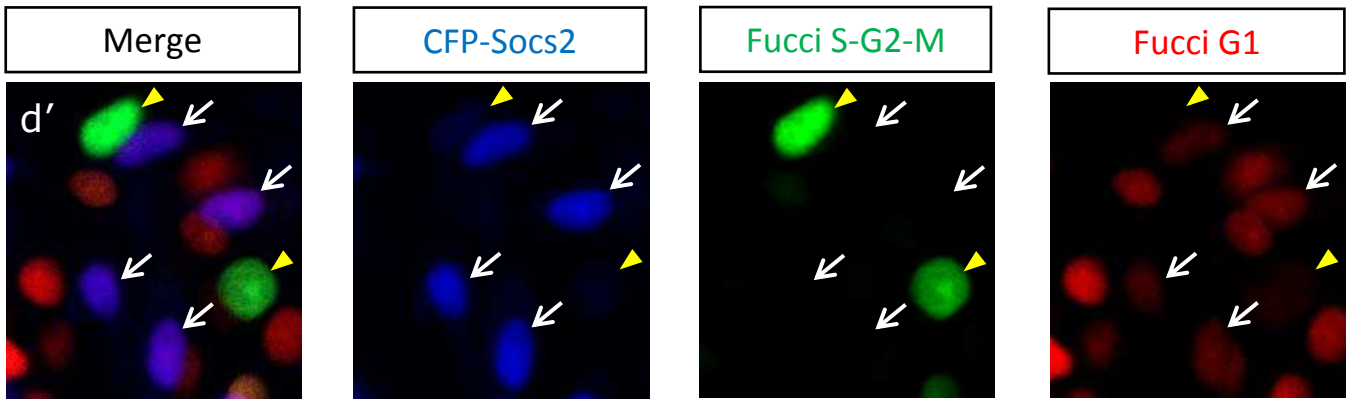
Merge
CFP-Socs2
Fucci S-G2-M
Fucci G1
d′

Figure 6 – figure supplement 1

Tg(ins:Renilla-mKO2);Tg(NF-kB:GFP) 3 mpf

a

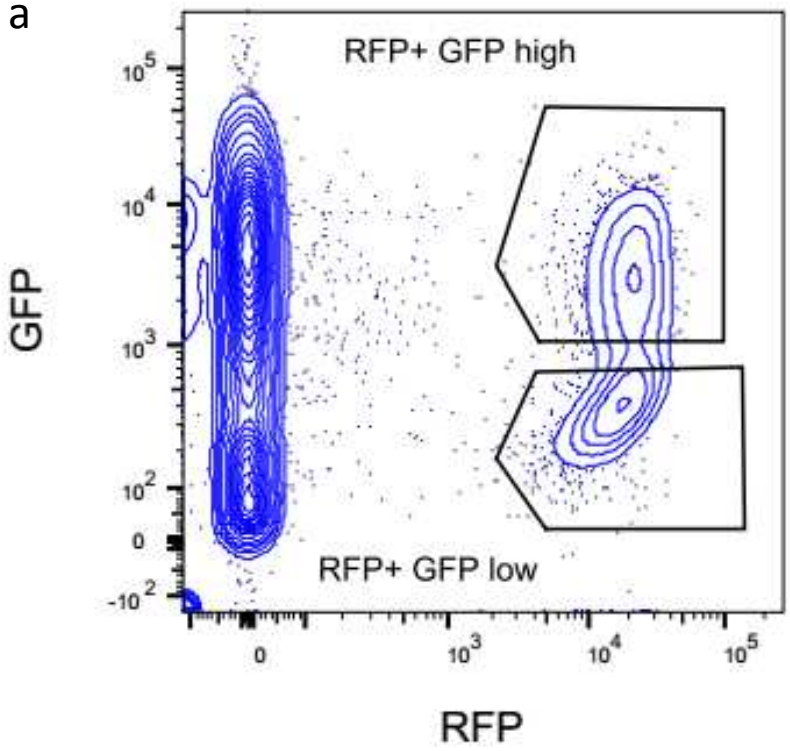

b

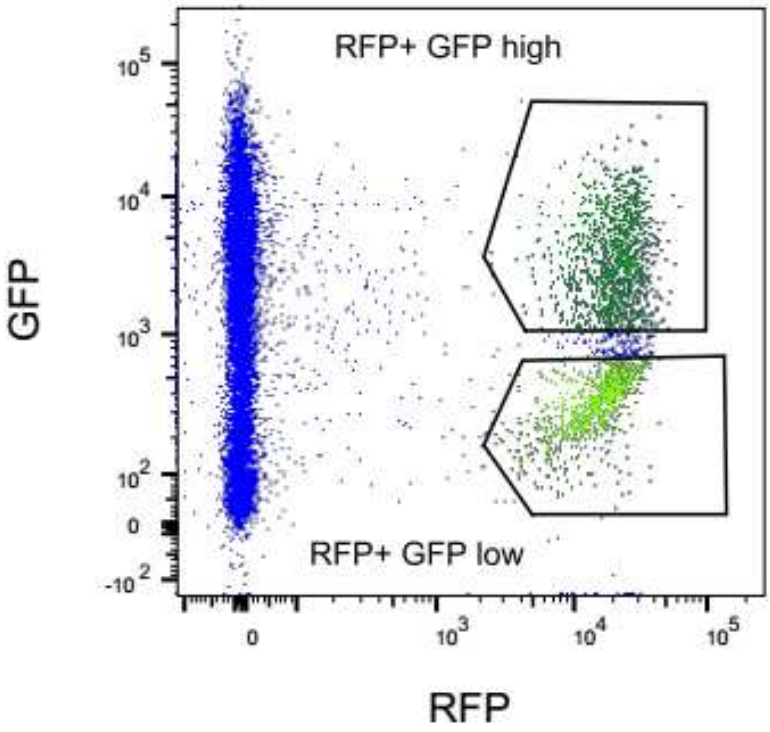

Figure 6 – figure supplement 2

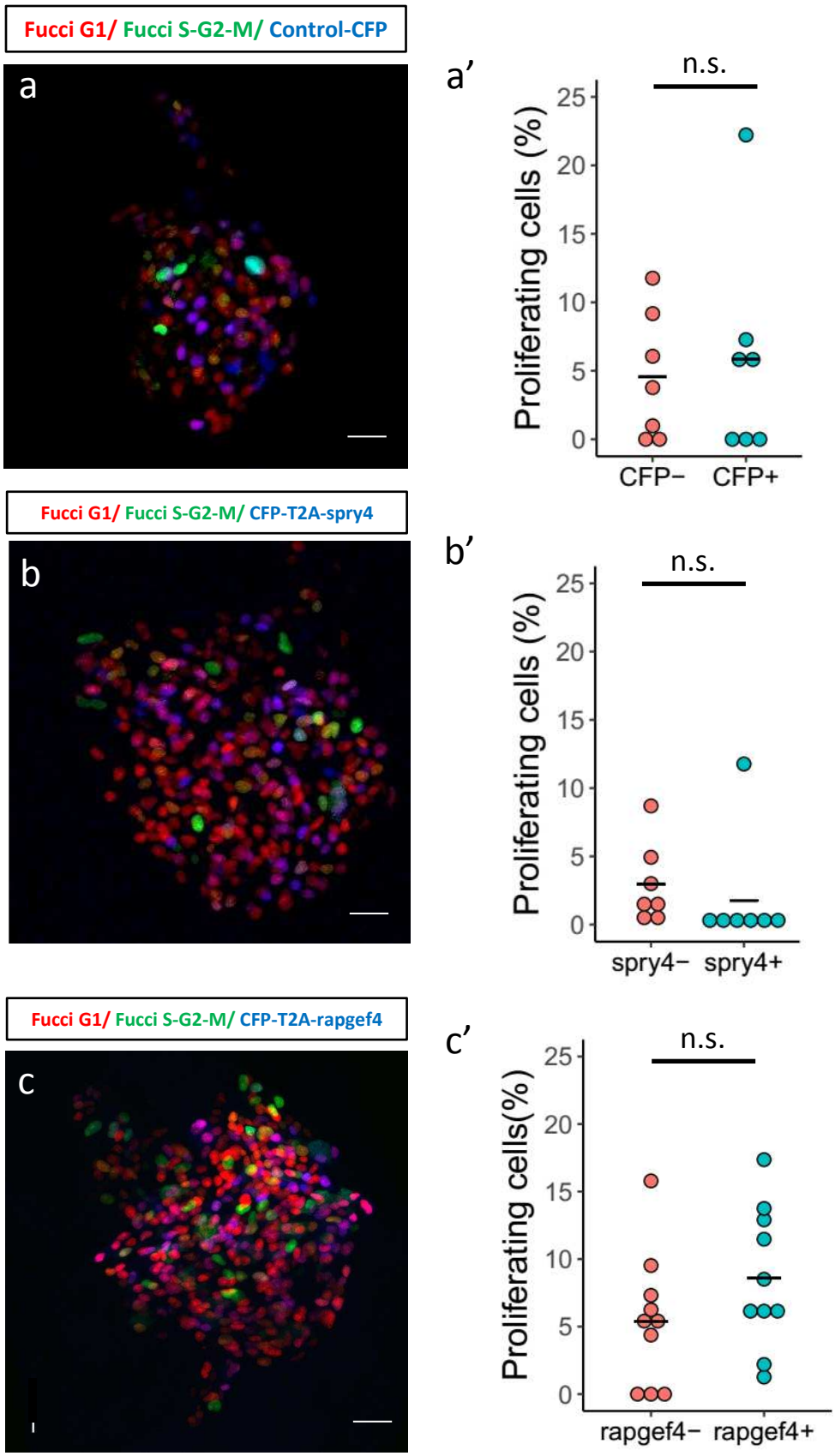

Figure 7

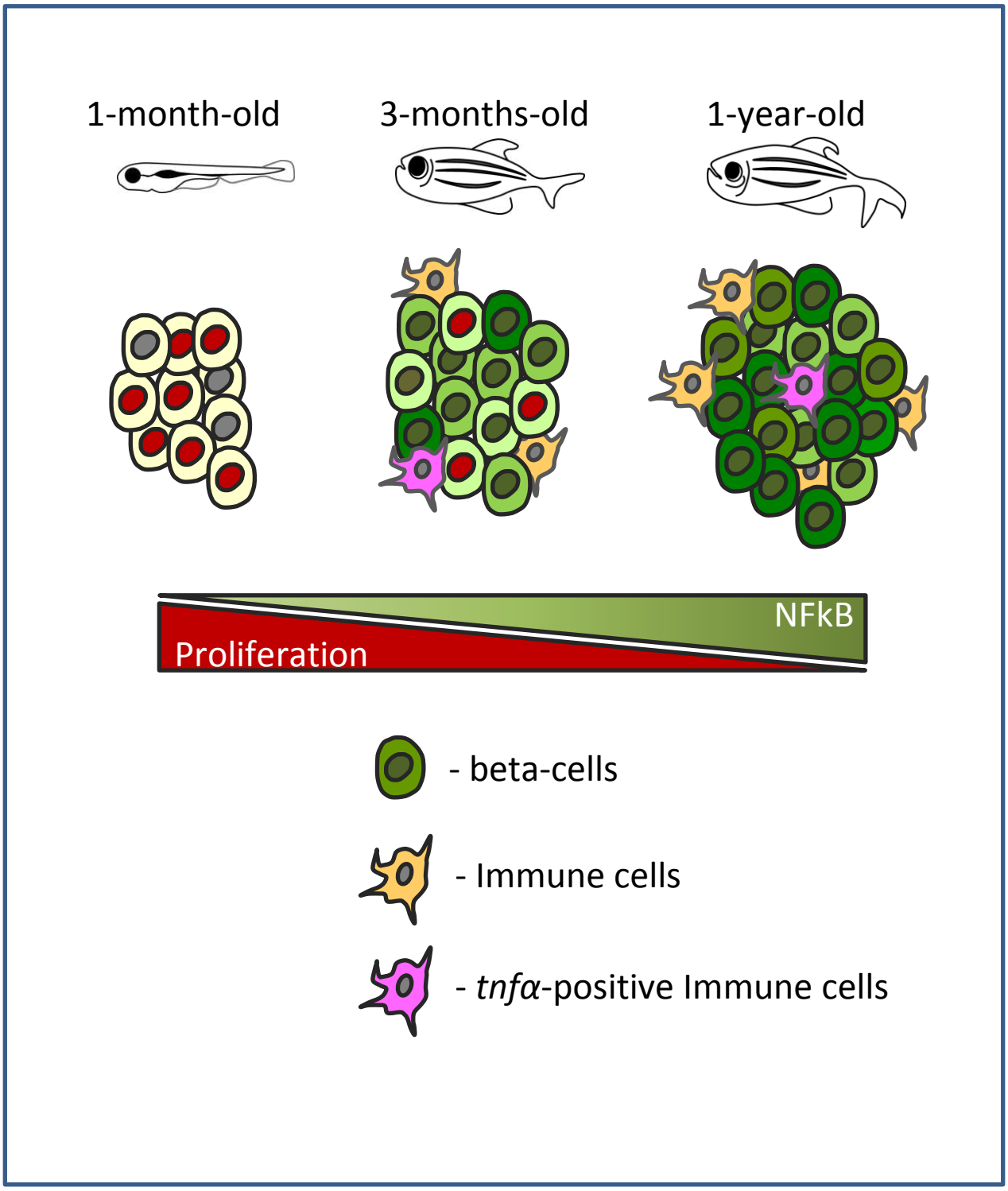
1-month-old
3-months-old
1-year-old
NFkB
Proliferation
- beta-cells
- Immune cells
- *tnfα*-positive Immune cells